Monitoring and Synchronization of Cardiac and Respiratory Traces in Magnetic Resonance Imaging: A Review

Martina Ladrova, Radek Martinek, Jan Nedoma, Pavla Hanzlikova, Michael Douglas Nelson, Radana Kahankova, Jindrich Brablik, and Jakub Kolarik

(Methodological Review)

***Abstract*—Synchronization of human vital signs, namely the cardiac cycle and respiratory excursions, is necessary during magnetic resonance imaging of the cardiovascular system and the abdominal cavity to achieve optimal image quality with minimized artifacts. This review summarizes techniques currently available in clinical practice, as well as methods under development, outlines the benefits and disadvantages of each approach, and offers some unique solutions for consideration.**

***Index Terms*—Magnetic resonance imaging (MRI), cardiac magnetic resonance imaging (CMRI), MRI triggering, cardiac triggering, respiratory triggering.**

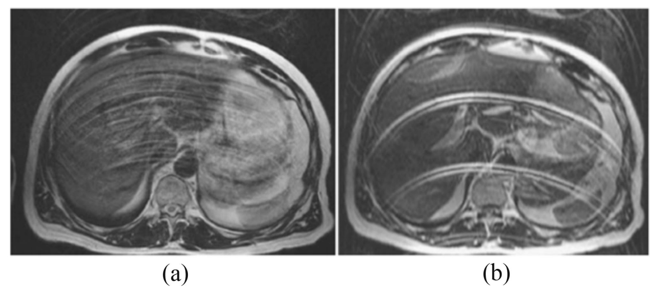

Fig. 1. Examples of MR motion artifacts: (a) blurring due to more random respiratory motion and (b) ghosting artifacts caused by periodic breathing [3].

I. Introduction

MAGNETIC Resonance Imaging (MRI) is a powerful non-invasive tool for imaging human body structure and function. The main advantages of MRI include the absence of ionizing radiation, high contrast between different types of soft tissues, and its ability to image in arbitrary spatial orientations. In addition to providing high-resolution images of the body structure, MRI also provides novel pathophysiologic insight into basic bodily functions (e.g., molecular water diffusion, tissue perfusion, or MR spectroscopy). Together, the information provided can help make more accurate diagnoses, and improves our ability to monitor treatment outcomes [1].

This review focuses on MRI applications that require vital sign synchronization, namely with the cardiac cycle and/or respiratory excursions. Indeed, triggering and gating devices and algorithms are necessary to ensure high image quality of regions within the chest and abdomen (e.g. heart, liver, pancreas). The task is to perform imaging during minimal movement of the heart and thorax, which causes motion artifacts, appearing as shadows or blurred contours on the image (referred to as "ghosting artifacts" see Figure 1). Synchronization serves to suppress these artifacts but is not without several major challenges. In particular, synchronization of biological signals is limited by inherent high-frequency disturbances and extreme magnetic induction, which interferes with the measurement of vital signs, and ultimately compromises MRI sequence synchronization [2], [3].

A. Abdominal MRI

Abdominal MRI is widely used due to its ability to extract information at the level of tissue composition and to assess functional status, including the metabolic structure of the tissue. It allows clinicians to respond to tissue damage or dysfunction and to adapt the therapy or disease prevention strategy accordingly. Given the versatility of MRI, it can detect a plethora of abdominal disorders, such as steatosis, fibrosis, inflammation,

Manuscript received August 28, 2020; revised December 22, 2020; accepted January 25, 2021. Date of publication January 29, 2021; date of current version January 24, 2022. This work was supported in part by the European Regional Development Fund in the Research Centre of Advanced Mechatronic Systems project, under Project CZ.02.1.01/0.0/0.0/16 019/0000867 within the Operational Programme Research, Development and Education, and in part by the Ministry of Education of the Czech Republic under Projects SP2020/156 and SP2021/32. *(Corresponding author: Radana Kahankova.)*

Martina Ladrova, Radek Martinek, Radana Kahankova, Jindrich Brablik, and Jakub Kolarik are with the Department of Cybernetics and Biomedical Engineering, Technical University of Ostrava, 70800 Ostrava, Czechia (e-mail: martina.ladrova@vsb.cz; radek.martinek@vsb.cz; radana.kahankova@vsb.cz; jindrich.brablik@vsb.cz; jakub.kolarik@vsb.cz).

Jan Nedoma is with the Department of Telecommunications, Technical University of Ostrava, 70800 Ostrava, Czechia (e-mail: jan.nedoma@vsb.cz).

Pavla Hanzlikova is with the Ostravska Univerzita, 70103 Ostrava, Czechia (e-mail: pavla.hanzlikova@osu.cz).

Michael Douglas Nelson is with The University of Texas, Arlington, TX 76019 USA (e-mail: michael.nelson3@uta.edu).

Digital Object Identifier 10.1109/RBME.2021.3055550

and tumors (malignant and benign). For example, when examining the liver, bile ducts, and pancreas, MR cholangiopancreatography begins to replace the invasive endoscopic method in diagnostic indications. Also, MRI can be used to identify inflammatory or neoplastic diseases with bowel wall abnormalities to classify some types of Crohn's disease by accurate detection of individual lesions and evaluation of disease activity. Moreover, MRI is also an excellent tool to differentiate the benign nature of asymptomatic adrenal lesions, the probability of which increases with higher age and is becoming a common problem. Clinical evaluation with MRI also plays a crucial role in the diagnosis, planning, and assessment of treatment of both benign and malignant gynecological conditions, and has even proved to be superior to computer tomography in the diagnosis of uterine and cervical cancer [1], [4].

B. Cardiovascular MRI

Cardiovascular magnetic resonance imaging (CMRI) is increasingly used to examine heart structure and function. Its non-invasive nature, together with its avoidance of ionizing radiation, allow for repeatable, low-risk characterization of the myocardium and its associated components, throughout disease progression/regression. One of the most frequent applications of CMRI in clinical practice is the assessment of atrial and ventricular morphology. Due to CMRI's high spatial resolution, three-dimensional coverage, and excellent high contrast-to-noise ratio (CNR), evaluation of chamber dimension, size and shape is highly robust and reproducible [5]–[7]. As such, CMRI is recognized for its accurate characterization and detection of cardiomyopathies (hypertrophic or restrictive cardiomyopathy, etc.), paracardiac masses (both malignant and benign cardiac tumors including secondary tumors, pseudotumors and intracavitary thrombi), congenital heart diseases, and conditions of the pericardium, septal defects, obstructive lesions, postoperative states and more. Cardiovascular MRI also includes structures beyond the heart, including the aorta and other major blood vessels. For example, MRI can be used to detect aortic aneurysm and dissection, as well as atherosclerotic plaque [5], [6], [9].

Synchronizing CMRI with the cardiac cycle provides additional insight into cardiac function and myocardial viability, allowing examination of myocardial ischemia and/or acute/chronic myocardial infarction. Integration of CMRI with velocity/flow measurements provides insight into cardiac hemodynamics and/or valvular function, such as mitral, tricuspid and pulmonary inflow versus regurgitation, valvular stenosis, pulmonary hypertension, or prosthetic valve function [5], [8], [9]. Furthermore, as CMRI has evolved, particularly over the past 10-15 years, more novel applications have emerged, including MR angiography, myocardial tissue characterization, and myocardial perfusion imaging [10]–[12].

C. High-Field MRI

There is a general trend in the field of MRI to increase magnetic field strength. In just the past 10 years, we have witnessed an extensive expansion of clinical scanners from 1.5 T to 3 T, with two of the major vendors now offering FDA-approved 7 T clinical scanners. In principle, increasing the magnetic field strength is directly associated with increasing signal intensity; however, it brings other sources of error. With the higher magnetic field strength, the inhomogeneity both of magnetic and radiofrequency field contribute to the degradation of image quality, which has to be reclaimed by different optimization techniques [13]–[16]. Thus, before the increased signal intensity and isotropic resolution can be realized, sophisticated algorithms must first be developed and integrated. Another limitation of imaging in high magnetic fields are the magnetic effects on the electrical signals used for monitoring vital signs of the patient; challenging synchronization (see more in Section II-A). Together, these inherent limitations often lead to prolonged scan times, and in some cases, impracticable long breath-hold times [17], [18].

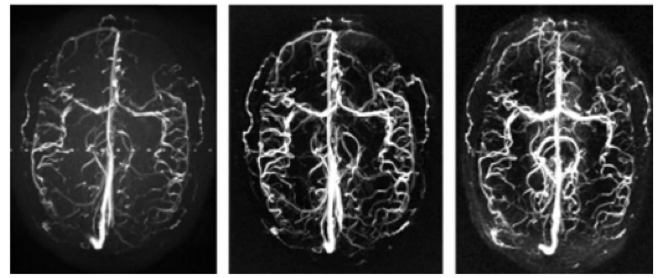

(a) (b) (c)

Fig. 2. Comparison of the quality of cerebral angiography images at (a) 1.5 T, (b) 3 T, and (c) 7 T magnetic field strengths [8].

Nevertheless, imaging at higher field strengths holds great promise. The contrast between blood and tissue is much more resolved, and there is great potential for accelerated imaging and reducing imaging artifacts; major advantages when imaging small, fast-moving structures [8], [19]. For example, the increased signal energy has a great advantage in MR angiography, where tiny vessels, such as cerebral arteries, are more visible at 7 T than at 1.5 T (see Figure 2). In this context, high field strength MRI promises to provide new insight into previously unresolved anatomical structure and physiological function *in vivo* [8], [18].

D. MRI Synchronization

Synchronization of MRI (or gating/triggering) is dependent upon real-time acquisition of cardiorespiratory function. As such, MRI gating can be divided into two main categories:

- *respiratory,* which allows reducing motion artifacts in the image resulting from the chest movement during a patient's free breathing (when scanning of an abdominal and thoracic area), and
- *cardiac,* the goal of which is to eliminate the effect of myocardial movement and capture a heart scan in the specific phase of its cycle (when scanning of a thoracic area), usually monitored by electrocardiography (ECG) signal.

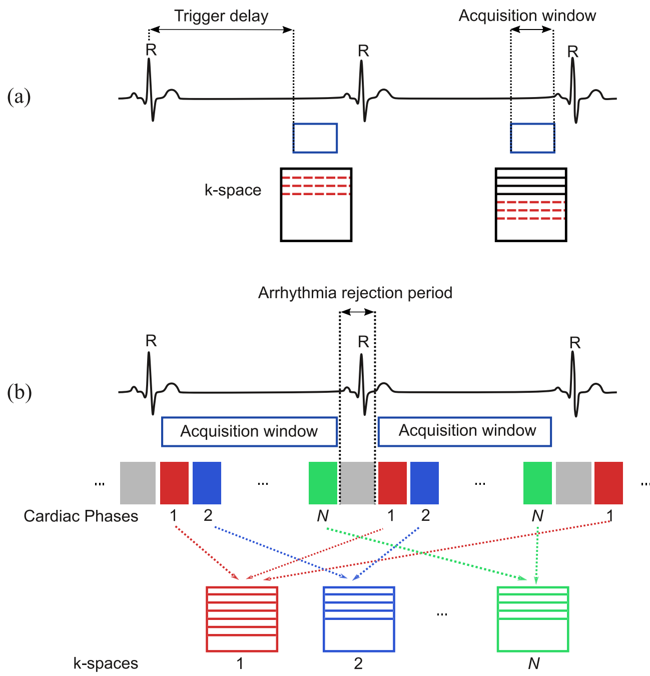

Fig. 3. The basic principle of the prospective triggering for (a) morphological imaging, (b) cine imaging.

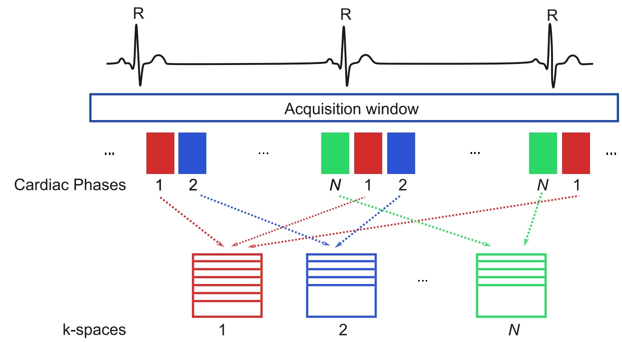

Fig. 4. The basic principle of the retrospective gating.

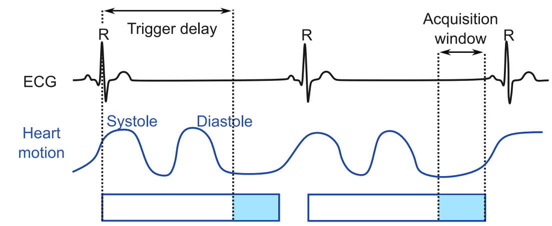

Fig. 5. The principle of cardiac triggering.

Synchronization of MRI can be divided into two basic principles ”prospective and retrospective. In the case of prospective triggering, the MRI acquisition is triggered by the desired physiologic event (e.g. R wave of ECG signal) with a specific delay or by reaching the specified level of inspiration. Thus, the acquisition usually coincides with the most mechanically quiet phase of the cardiac/respiratory cycle (see Figure 3) [20].

Prospective triggering in cine imaging allows data acquisition covering most of the cardiac cycle, determined by the number of cardiac phases or segments within an R-R interval. The acquired data are sorted into k-spaces (representing the individual frames) according to the cardiac phase, and each k-space is filled over several heart beats. This functional set starts with the R wave. Since the duration of the R-R interval varies slightly from the heartbeat to the end, the last 10% of the R-R interval is usually not sampled (see Figure 3(b)). Prospective triggering has advantages in noise filtration.

The interval of acquisition is often set such that the detector intentionally ignores any high amplitudes other than R waves, preventing false triggering. This ability, however, is problematic when monitoring patients suffering from rapid or irregular activity ”arrhythmias. In patients with premature heartbeats, the earlier R wave is passed because the gradient pulses triggered by the previous R wave are still running, which results in extended acquisition time. This heart rate variability must be considered when planning the acquisition window positioning for a prospectively triggered examination. For the detection of the next R wave, the acquisition window position should not be too close to the next R wave. An acquisition window placed too close may interfere with the next R wave and shorten the corresponding R-R interval. During the scan, the examiner must monitor changes in the heart cycle and appropriately adapt the triggering parameters [21], [22].

Retrospective gating allows continuous acquisition of MR data (see Figure 4). Both the image and the heart/respiratory signal are captured over several cycles and used to reconstruct the image by reordering, grouping, or correlating with phase of the cardiorespiratory cycle. This procedure requires unconventional “real-time” pulse sequence (e.g., for functional imaging) and acquisition software decisions, because the method of data acquisition changes as it runs. In this way, retrospective gating uses complex methods for interference filtering [20], [21].

The main advantage of retrospective acquisition is the ability to collect data from all heart phases. Like prospective triggering, retrospective methods may have problems with arrhythmias and low R-wave amplitudes. The systolic and diastolic periods are unevenly altered in case of heart rate variability or arrhythmia events, so retrospective software is unable to compensate by appropriate data segmentation, resulting in error [21], [22].

The following chapters outline common problems related to cardiac cycle and respiratory synchronization, summarize available synchronization techniques commonly used in clinical practice, as well as introduce several novel synchronization approaches currently under development. We discuss the advantages and disadvantages of each approach, especially in the case of the increasingly popular high field strength MRI.

II. Cardiac Gating Methods

Cardiac gating is critically important for CMRI. In current practice, cardiac activity is most commonly monitored by ECG signal. The principle of cardiac triggering (see Figure 5) is based on the detection of a change in signal of the heart (e.g., the R wave of ECG signal, ventricular depolarization). Given the prominence of the R wave, and its routine use in cardiac

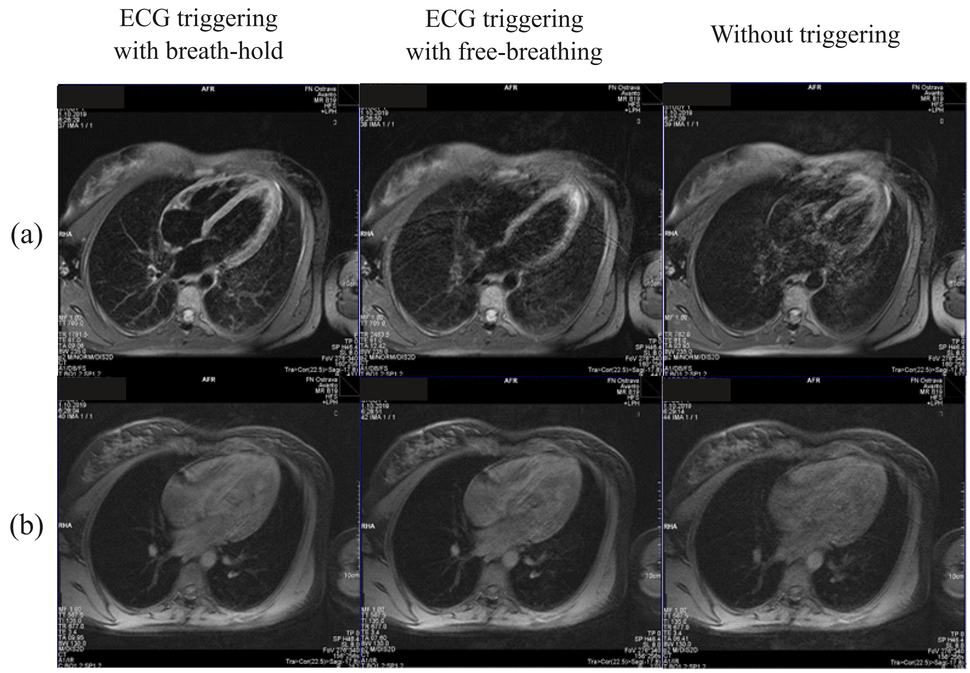

Fig. 6. Comparison of ECG-triggered and non-triggered images using (a) T2-Weighted Fat-Suppressing Sequence, and (b) T1-Weighted Myocardial-Suppressing Sequence.

physiology to denote the beginning of the cardiac cycle, cardiac imaging is often triggered by the R wave [23]. Depending on the imaging being performed, detection of the R wave may initiate a series of evenly timed acquisitions across the R-to-R interval in order to reconstruct a cinematic image of cardiac systole and diastole. Alternatively, the R-wave may be used to define the time period of a single acquisition (e.g. end-systole or mid-diastole).

The most commonly used heart scan sequences are cine T1/T2-weighted sequences, fat-suppressing T2-weighted sequences, and myocardial-suppressing T1-weighted sequences. These examinations are usually performed under respiratory quiescence, with the subjects holding their breath for the entire measurement period "from 6 to 25 seconds "to avoid respiratory movement artifact. Figure 6 shows examples of scans triggered by combination of ECG signal and a breath-holding/free-breathing. As can be appreciated, combining ECG triggering with respiratory quiescence improves overall image sharpness and eliminates motion artifacts.

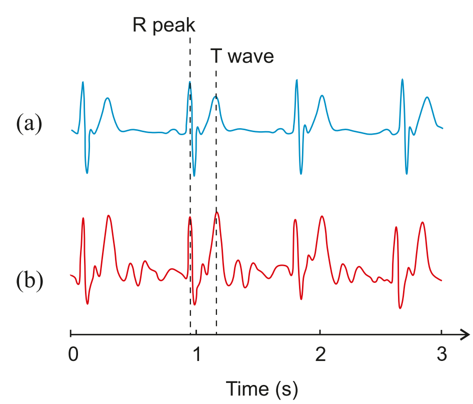

Fig. 7. Demonstration of magnetohydrodynamic artefact affecting ECG waveform measured: (a) outside the influence of MR magnetic field, (b) in the 1.5 T magnetic field, where both the R wave and the T wave acquire similar amplitudes.

A. Cardiac Gating Challenges

Artifacts during MRI may originate from both the patient and the measurement system. Firstly, the electrodes and associated connectors and cables should be made of non-ferromagnetic material to reduce magnetic field distortion, whereas interference may falsely trigger the scanner and cause loss of synchronization with the heart [21], [24]. Blood flow in the heart can induce voltage and generate hydrodynamic artifacts. Since blood is an electrically conductive liquid whose movement produces an electrical current added to the heart signal, a magnetohydrodynamic effect occurs. The electrical signal generated in this way usually affects the T wave of ECG signal (see Figure 7). If the T wave occurs at a time of rapid movement of blood from the heart, the T wave is distorted [25]. In addition, surface receiver coils are commonly used in CMRI examinations to amplify and improve the acquired signal, causing this interference to increase significantly.

Other problems, such as disorders of cardiac conduction system or unrelated physiological processes (e.g., muscle tremor), are additive to the interference mentioned above. The optimal image quality requires appropriate electrode placement that maximizes the amplitude of the R-wave while minimizing these fundamental artifacts. Extreme changes, such as the noise of a high-amplitude gradient system or the small electrical currents caused by a change of magnetic field gradient, are very disruptive. However, due to the large frequency difference between

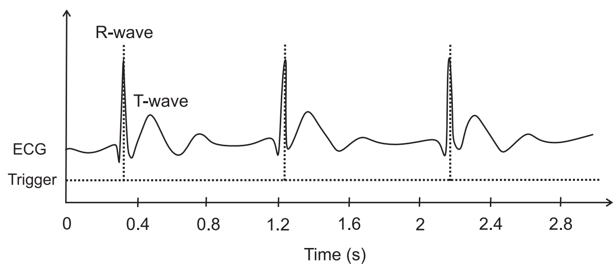

Fig. 8. ECG waveform with its triggering signal.

the noise and ECG, high frequencies can often be suppressed by filtering [21], [26].

In many applications, both prospective and retrospective rejection of arrhythmia has been integrated into acquisition and reconstruction software. In this case, an acceptance window that allows R-R variability must be specified. This step usually increases the acquisition time, and the examiner has to decide whether to reduce the scan time by increasing the number of segments at the expense of image quality. However, the use of prospective gating instead of retrospective gating can overcome extreme deviations of the R-R interval. Typically, the shorter R-R interval should be used to schedule the acquisition window, which must be slightly shorter than the shortest R-R interval. The resulting image will represent an incomplete heart cycle, but a calculation of ejection fraction (among other outcome measures) is still possible [21], [24].

The artifacts related to magnetic field are particularly pronounced during measuring at high magnetic field strength. When using field strengths higher than 3 T, the influence of the magnetohydrodynamic effect on the signal increases, and obtaining a clear signal of sufficient quality for faultless triggering becomes more difficult [27], [28]. As ultra-strong MRI fields become more widespread, solutions to this sensitivity issue are increasingly needed. Thus, new methods of triggering CMRI, discussed in more detail below, have been developed and are currently being studied.

B. Electrocardiography

Sensing of the ECG signal (see Figure 8) is one of the best known and most commonly used methods of monitoring cardiac activity. The ECG measurements consist of placing the electrodes on the patient's chest at the specific locations. It is measured in current leads, usually in 12 leads for standard non-MR diagnostic measurements with 3 limb electrodes included. When triggering CMRI, fewer leads are sufficient, because the signal does not serve as a tool for a diagnose of the heart function disorders but only of the QRS complexes detection. Thus, the number of electrodes is commonly reduced to three or four (see Figure 9) [24].

Although ECG is a means of quick cardiac function recording from which each phase of the cardiac cycle can be determined for the purpose of MRI triggering, many problems with the MRI device itself and its magnetic field, such as artifacts or complications when measuring with certain materials, arise. For the best possible prevention of artifacts, it is necessary to

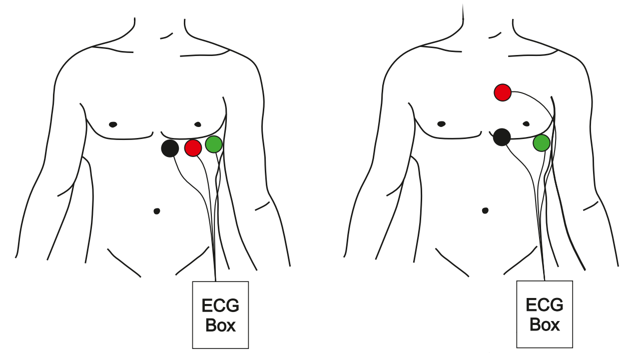

(a) (b)

Fig. 9. Typical distribution of ECG electrodes in MR environments: (a) – parallel distribution advantageous for high magnetic field strengths, (b) – electrode distribution normally used at 1.5 T field strengths.

(a) (b)

Fig. 10. Example of available ECG-based sensors: (a) Wireless ECG unit for sensing in MR environment [32]. (b) Quadtrode ECG electrode for the MR gating [33].

prepare the skin well at the locations of ECG electrodes (most often floating electrodes) placement, since accurate detection of low potentials requires minimal skin impedance and optimal electrode contact with the skin. The added noise that results from poor electrode contact with the skin then leads to erroneous triggering during the CMRI examination. Immediately before the examination, the hair must be shaved, and the skin surface scrubbed off with a mild abrasive soap or gel before electrodes are applied; complicating the exam and adding discomfort to the patient [20], [21].

Furthermore, ECG measurements require some safety precautions due to the interaction of the ECG system with RF and gradient systems, since ECG, as a measurement with electrically active components, brings the risk of superficial heating of the patient's skin or even burns resulting from high voltage induction in ECG hardware [29], [30]. To prevent currents occurring in the ECG leads due to the rapid switching of gradient fields, the location of the leads has to comprise no loops, and the wires should be as short as possible. The possibility of burns due to interaction with the RF field should be reduced by location of the wires outside the resonators, and the battery-powered ECG measuring unit (see Figure 10(a)) should be used to ensure galvanic separation of the MR system and the patient [31].

All of the major MRI vendors offer ECG gating products, and several commercially available products are also available through third party vendors. Modern products include MR-compatible 3-lead ECG triggering device using a secure fixed electrode layout (see Figure 10(b)), which restricts cable length by dictating a tight electrode placement pattern and thus,

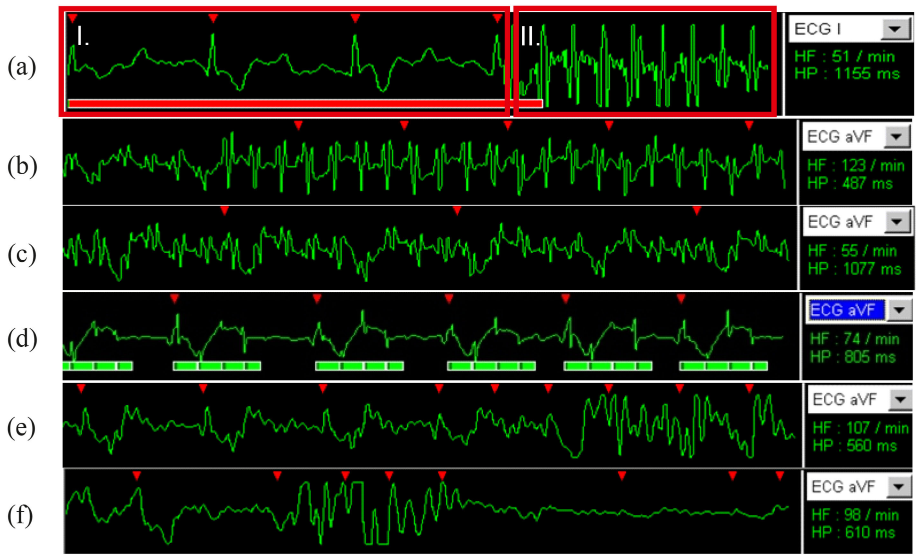

Fig. 11. The example of the ECG waveform for cardiac triggering: (a) before (I) and after (II) sequence start, (b) and (c) during the acquisition with failed triggering, (d) during the acquisition with successful triggering, (e) with improperly positioned ECG electrodes, (f) with motion artifacts.

provides optimal signal performance and safety due to large electrode contact area. This new design significantly lowers resistance using the unique gel, and reduces at least partly patient preparation time and discomfort thanks to its form of disposable patch [33]. Several commercially available systems allow measurements of more vital signs together, such as ECG, respiratory function and blood pressure, so that provide a detailed information about patient's condition during examination [34].

As described above, it is also important to consider the influence of magnetohydrodynamic effects during ECG synchronization. This effect causes ECG signal distortion and prevents a proper detection of R wave and subsequent synchronization. For example, Krug *et al.* [35] and Snyder *et al.* [36] have shown that ECG triggering is not appropriate for high fields. At field strengths beyond 3 T, the ECG recording is both spatially and temporally distorted, to the point that the R wave may no longer be clearly identifiable or overshadowed by the T wave dominance, exceeding the R wave by 20% of its amplitude. Indeed, the amplitude of the T wave can even be augmented at field strengths as low as 1.5T [37], challenging translation of ECG monitoring/synchronization at higher field strengths. While the prevalence of this problem remains incompletely understood, some reports estimate the problem to exist in as many as 30% of cases [27], [38]. This is particularly troubling, given the importance of accurate R wave registration for image acquisition [27], [28], [39].

Figure 11 shows examples of the ECG signal within examination with various deformations that prevent proper synchronization. To clearly demonstrate the effects of the MR environment on the ECG signal, Figure 11(a) shows the ECG signal prior to initiating a scan sequence (I), and during acquisition (II). Note how the ECG signal is distorted by the RF pulse during acquisition, preventing R wave delineation, similarly to other cases in Figure 11(b) and Figure 11(c), when only several R waves were detected. The correct trigger signal obtained from the distorted ECG during acquisition is only achieved in Figure 11(d). Figure 11(e) shows an example of low amplitude R-waves lost in the baseline noise and thus, their failed delineation. It is caused by poor electrodes cleaning and sticking, insufficient shaving, and improper positioning of electrodes. Motion artifacts are denoted in Figure 11(f), when the signal is completely distorted, and R waves are not detectable.

For all these reasons, more advanced methods of R wave detection and magnetohydrodynamic artifact suppression have been developed and used, such as noise cancellation [40], independent component analysis [41], [42], nonlinear Bayesian filtering [42], wavelet transform [44] or their combinations. For example, Abi-Abdallah *et al.* [45] proposed signal decomposition using wavelet transformation and subsequent adaptive filtering. For this approach, an off-line wavelet transformation process is made to eliminate the delay in signal filtering as much as possible, generating a reference signal that can be used with an adaptive filter during the real-time calculation phase. The algorithm also calculates the respiratory synchronization signal by extracting a breath waveform that modulates the ECG signal. Then, a combination of both heart and respiratory triggering signals performs MR synchronization.

More modern approach includes a real-time higher-order QRS detector based on adaptive thresholding [46]. The threshold uses a fourth central moment calculation that represents a significant signal change within the QRS complex compared to other components, such as the T or P wave. Stäb *et al.* [47] observed only rare occasions of false negative, false positive or misplaced trigger events of ECG triggering at field strength 7 T by including a learning phase for the R-wave detection. The proposed trigger algorithm learns the shape of the rising edge of the R-wave while the subject is lying outside the magnet bore, where the magnetohydrodynamic effect is negligible. After learning phase is completed, the algorithm compares different derived entities of the incoming ECG signal with the corresponding entities of the learned shape in real time.

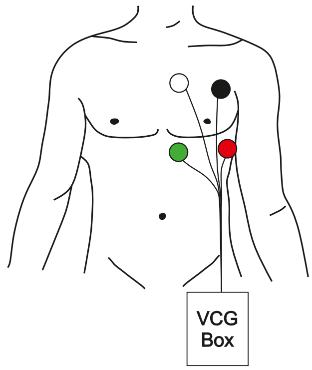

Fig. 12. Typical placement of VCG electrodes in MR environment.

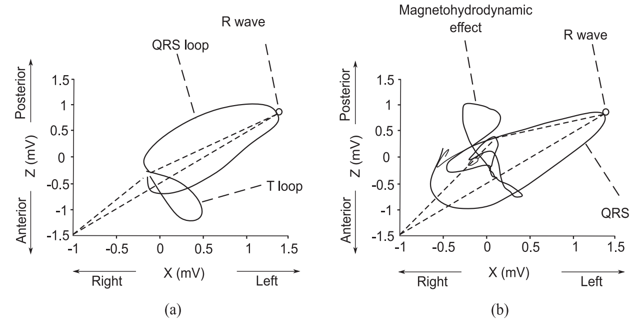

Fig. 13. (a) Typical VCG waveform and (b) manifestation of magnetohydrodynamic effect.

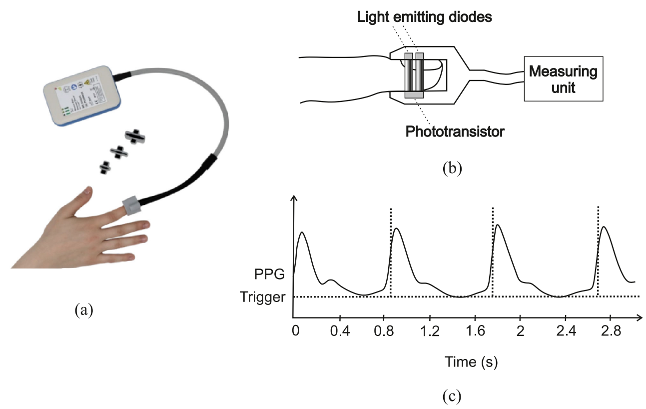

Fig. 14. Illustration PPG based system principles and deployment: (a) Example of finger PPG unit for measurement in MR environment [32], (b) Principle of PPG signal sensing from finger, (c) PPG waveform with its trigger signal.

Although the discussed methods, improving the R wave delineation, reached very high accuracy in cardiac triggering, the processing algorithms have unduly high computational requirements and have not been yet suitable for introduction into the medical practice. The insufficient computing performance in the past was the main limiting factor for using these complex methods, which remained to be used only in the research area. However, the increasing performance of microprocessor technology (multicore processors, programmable gate arrays, etc.) brings new trends and possibilities in available computer equipment, signal processing and analysis over the past few years. On the other hand, although the software improvement of ECG synchronization does not demand the additional hardware, the research of other sensing methods (working on another physical principle) could increase the accuracy of cardiac synchronization right in the lowest sensory layer. Thus, together with advanced processing algorithms, they could provide higher image quality for diagnostics.

C. Vectorcardiography

Vectorcardiography (VCG) describes electrical activity of the heart by three independent loops, each representing individual phases of the cardiac cycle (P wave, QRS complex, and T wave). The loops can be displayed in a one-dimensional image, similar to the conventional ECG, as well as two- and three dimensional loop reconstructions, represented by the amplitude (mV) of the electrical signal between leads (i.e. X, Y lead; X, Z lead; Y, Z lead; or across each of the X, Y, and Z leads). In terms of diagnostic information, VCG is more sensitive for the detection of hypertrophy and ischemic heart disease [48]–[51]. In the MR environment, VCG is more resistant to the magnetohydrodynamic effect, since the heart's electrical axis is oriented in the opposite direction of blood flow through the heart. For this reason, some studies have begun to investigate CMRI synchronization using the VCG instead of the ECG signal, where the vector model is used to approximate the ECG signal from any lead. From an application perspective, the main difference between ECG and VCG resides in the placement of the electrodes attached to the patient's chest (see Figure 12).

As mentioned, VCG has gained in popularity within the MR community, given its resistance to the magnetohydrodynamic effect (see Figure 13). Indeed, its utility for cardiac synchronization has been recognized for more than two decades, with a degree of success [24], [26], [52]. Like ECG monitoring, however, the method lags in cases of severe arrhythmia, when the triggering system is unable to differentiate the QRS loop from the loop generated by the ectopic beat. Likewise, VCG is similarly affected by high strength and complexity of the magnetohydrodynamic signal in 7 T field strength [35].

D. Pulse Wave

Cardiac synchronization using a peripheral pulse measured by photoplethysmography (PPG) is not as widespread as a standard ECG signal measurement but is a suitable alternative, especially given its resistance to MR artifacts. The PPG signal (see Figure 14(c)) is most often measured by a light sensor (see Figure 14(a)), which works by assessing the blood absorption of light corresponding to changes in blood volume (see Figure 14(b)). The rise and fall of this measured wave reflect the systole and diastole process, making it a suitable tool to trigger CMRI [53]. While pulse wave detection is technically simpler, involving placement of a device on an easily accessible finger (as oppose to electrodes placed on the chest), several major disadvantages have prevented its widespread adoption for routine MR synchronization. First, the light sensor is susceptible to movement, especially movement of the finger/hand on which

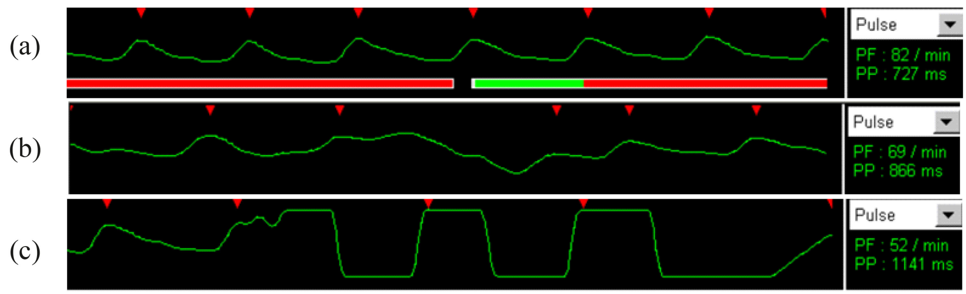

Fig. 15. Pulse waves with triggering marks (a) signal without artifacts, (b) signal with artifacts caused by the moderate movement of the finger, (c) signal distorted by strong and sharp movement.

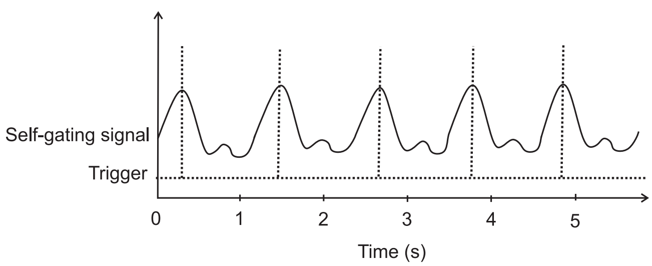

Fig. 16. Self-Gating waveform with its trigger signal.

the sensor is located. Figure 15 illustrates typical movement artifact, and the associated triggering error that accompanies such movement. Spicher *et al.* [53], [54] have attempted to overcome this limitation by introducing a contactless video-based PPG system, but have not yet succeeded in widespread clinical integration of this approach. Second, the delay between cardiac activity (i.e. mechanical ejection of blood) and detection of that activity in the periphery creates a sizable time delay (i.e. several hundred millisecond delay needed for pulse to travel to the periphery), the extent to which cannot be accurately, nor reproducibly corrected for [27]. Therefore, in most cases, this triggering method is only used when other triggering methods fail. The most notable exception is flow imaging of cerebrospinal fluid through cerebral ventricles and openings, for which PPG triggering is superior to ECG gating [55].

E. Self-Gating Methods

Self-gating (S-G) techniques, see [97]–[100], eliminate the need for extra hardware for CMRI synchronization by receiving the triggering information directly from MR signals. The method relies either on acquiring radial (or spiral) k-space data that cover the k-space center in each readout or on acquiring additional (non-phase-encoded) navigator readouts through the k-space center. This major advantage is not without its own drawbacks however, as such an approach significantly extends the scan time.

The principle of S-G CMRI is based on changes or movement of volume in the image. That means a series of consecutive echoes demonstrates peak alterations corresponding to proportional changes in total transverse magnetization due to organ movement and changes in blood volume. This data is then processed and segmented to create an ECG compensating signal (see Figure 16), according to which the image is subsequently reconstructed according to the associated cardiac cycle, represented by the amplitude and phase of the echo [97]. Due to its nature, this signal is resistant to artifacts that may affect triggering signals of other methods (ECG, VCG, etc.). The S-G method is based on a first-difference detection algorithm; however, many studies deal with more complex types to increase the accuracy of cardiac synchronization [99].

Nijm *et al.* [99] compared the classical method, based on the first difference calculation (including the signal filtering by its derivative), with more complex methods, such as the median template matching technique (with calculation of the correlation between the original signal and the template, determined by half the RR median calculated by the first difference method) and polynomial matching technique (a polynomial with length of an RR interval median is used as a template here). The cubic polynomial method achieved the lowest error and the highest SNR and was deemed "comparable" to ECG synchronization. It is worth noting however, that none of the S-G methods outperformed the ECG measurement technique or the original first difference method.

In order to eliminate efficiency deficits of the previously introduced S-G methods, the others include using modulation of MR echo that occurs through: (1) tissue movement itself (echo-peak method), (2) kymogram (1D gating signal from the temporally evolving 2D center of mass), and (3) 2D low-resolution image correlation [101]–[105]. In each case, the set of views at each cardiac phase was derived using time-stamp information and complex linear interpolation algorithm. A linear regression algorithm was used to compute signal components for individual sampled k-space positions (i.e., spatial-frequency domains) across cardiac phases. Then, the convolutional algorithm for image reconstruction created an image of each cardiac cycle. The delay of all obtained S-G signals is 2.5 ms. The echo-peak method seems to be the most practical of the three methods tested considering the image quality, values of the time variability of the triggering signal, and low computational cost. Moreover, the correlation technique requires an operator's interaction. All three methods achieved very similar results of image quality compared to ECG synchronization [97].

Most central line S-G methods results in a doubling of the acquisition time, while radial streak artifacts are encountered with the projection reconstruction method and can interfere with image interpretation. To overcome these limitations, Crowe *et al.* [100] utilized S-G triggering on a double-echo sequence where the second gradient echo without phase coding was used to generate a trigger signal. A sampling of the second echo provided subjective image quality score between good and excellent, which means a satisfactory resolution and contrast for image interpretation and definition of fine anatomic structures. Also, no statistically significant differences were obtained between S-G and ECG-gated images and mass parameters measurements in all volunteers at clinically practical acquisition times, extended negligibly. This technique is not susceptible to the radial streak artifacts, but there was no statistically significant difference in image quality between S-G and ECG synchronization.

Most S-G methods have been successfully used for retrospective gating of CMRI, which is not as sensitive to changes in heart rate (as in the case of prospective triggering) and provides an image throughout the heart cycle, which is particularly important for determining compulsive systolic or diastolic processes [99]. The S-G technique is unsuitable for prospective triggering, which requires accurate determination of trigger delay in order to place an acquisition window in the target phase of the cardiac cycle [28], [97], [99]. Furthermore, these methods are lagging in very high heart rate and some heart diseases expressing themselves by very mild myocardial contraction and relaxation throughout the heart cycle [100]. Hiba *et al.* [98] overcame this challenge of scanning at a very fast heart rate (up to 600 bpm) when testing the S-G echo-peak method during imaging a rat's heart. The S-G triggering provided better imaging of papillary muscles than ECG gating and achieved higher SNR values.

F. Optical Methods

The use of fiber optic sensors brings an innovative approach to biological signals measurement and is increasingly being handled by current research. Optical sensors enable sensing a wide range of signals, such as sound manifestations, pressure changes, or temperature variations. All these signals are measured non-invasively simply by attaching the sensor to the sensing location, e.g., a patient's chest or back. The optical measuring of vital signs in the MRI environment has the basic advantages of its harmlessness since the sensor is made only of optical fiber material and protective elements (cases). Moreover, the sensors are highly immune to the artifacts arising from magnetic and high-frequency electromagnetic fields, so no artifacts occur in the image. Other benefits include the very small dimensions of the sensors, their low weight, and the minimization of wires. However, the significant disadvantage of optical methods is the high cost and size of the interrogation and measuring unit, which allows the conversion of signals into digital format. On the other hand, this unit can be used to evaluate the results of multiple sensors. Thus, the price of the system can be decreased when comprised to the department with multiple MR scanners, which is usual in the clinical practice.

Today, the most commonly used types of optical sensors include sensors based on light interference, so-called interferometric sensors, and sensors with Fiber Bragg Grating (FBG), which evaluate changes of light reflected on the grating structure. The minor but currently evolving part consists of micro- and macro-bending fiber optic sensors, which work on the principle of evaluating changes in light output caused by optical fiber bends created through a "sandwich" micro-bender structure (see Figure 17) [56]–[58].

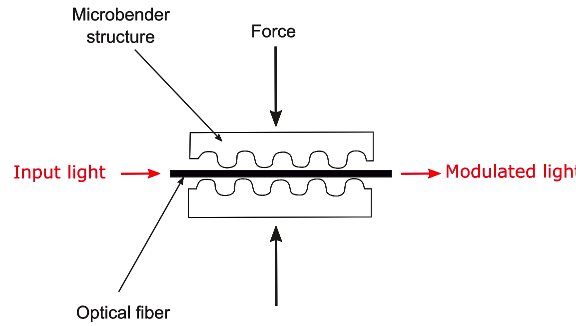

Fig. 17. Principle of micro-bending optical sensor. The device detects changes in the input light due to the mechanical action (force) on the optical fiber.

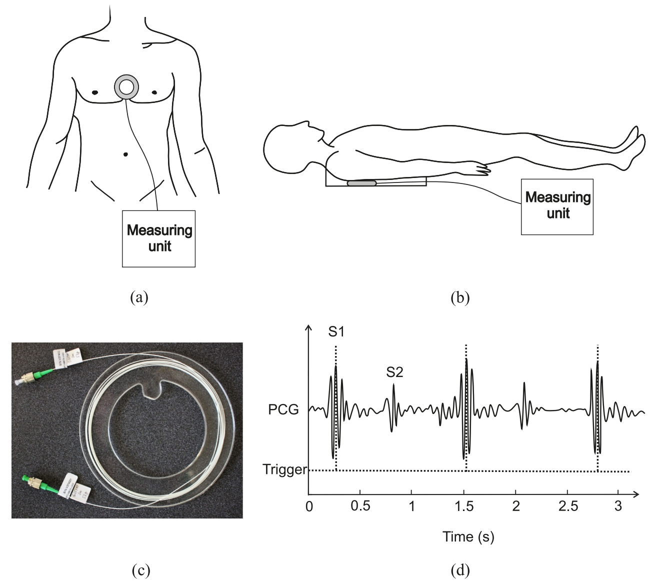

Fig. 18. Illustration of PCG based system principles and deployment: Typical interferometric sensor placement for the cardiac activity measurement in position: (a) " standing, (b) " supine; (c) Example of an Interferometric sensor (d). PCG waveform with its trigger signal.

The principle of measuring heart rate using interferometric sensors (see Figure 18(c)) is generally based on phonocardiography (PCG) signal (see Figure 18(d)), generally consisting of several heart sounds (S1 "S4). Still, in most cases, only the first two sounds are evident, of which the first (S1) reflects the ventricular systole. The mechanical-acoustic activity of the heart and the mechanical activity of the lungs cause changes in the refractive index of the core and in the length of the measuring arm of the sensor placed on the body (see Figure 18(a),(b)). The interferometric measuring system then evaluates these changes. This method of cardiac activity monitoring has indeed been described previously [59]–[67]. The principle of heart rate measurement using an FBG sensor is based on ballistocardiography (BCG, see Figure 19(d)) and has been described previously [69]–[76]. Cardiac activity is manifested physiologically in the chest area by a slight pressure action occurring due to the mechanical

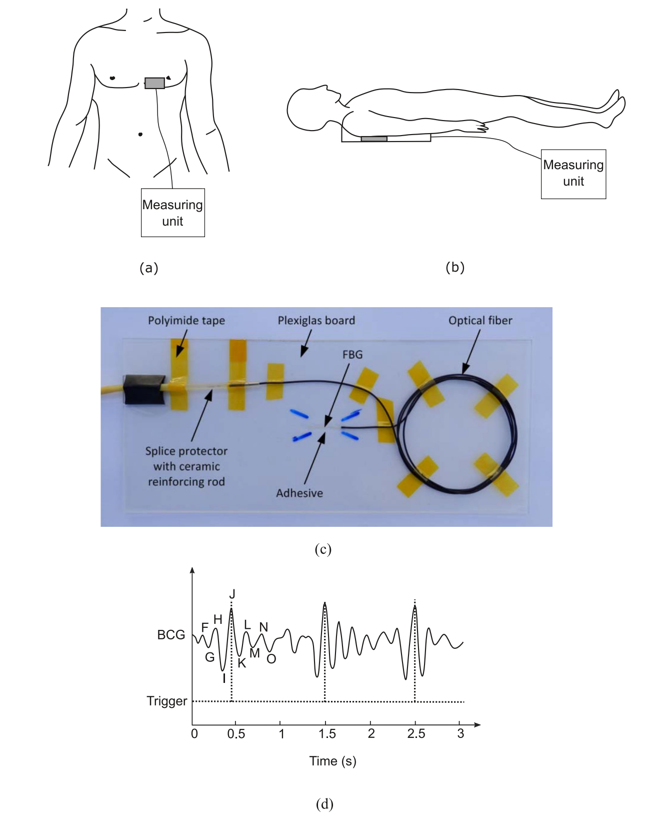

Fig. 19. Illustration of BCG based system principles and deployment: Typical FBG sensor placement for heart activity measurement in position: (a) “ standing and supine, (b) ” supine. Example of FBG sensor for the heart activity measurement [77] (c); BCG signal waveform with its trigger signal (d).

activity of the heart. This phenomenon causes pressure on the sensor located in the chest (heart) area of the human body (see Figure 19(a),(b)). A suitably positioned and encapsulated sensor (see Figure 19(c)) can detect these weak heart signals. The BCG signal generally consists of three phases: the pre-ejection phase (FGH complex), the ejection (IJK complex), and the diastolic part of the heart cycle (LMN complex). J-wave, as a reflection of rapid ejection of both ventricles and blood acceleration in the descending and abdominal aorta, is commonly used to detect heart activity [77]. Measurement of vital signs using FBG sensors within the MR environment has indeed been previously described [68], [74], [77]–[84], along with synchronization with the cardiac cycle specifically [82]–[84]. As mentioned, the major advantage of these sensors, especially FBG and micro-bending sensors, is the ease at which they can be integrated into clinical imaging; and the versatility of endpoint measurements that can be obtained [85]–[92]. For example, De Jonckheere *et al.* [85] implemented a measurement system into textile, which is placed around patient's chest or abdomen to monitor heart rhythm, respiratory movements, arterial pulse waves, and oxygen saturation. Chen *et al.* [93] created a sensing pad using micro-bending sensors that can be built into a mattress, chair or pillow with wireless transmission to a computer, showing accurate heart rate detection ($<1\%$ error related to pulse oximetry reference sensor), even in the 3 T environment.

Nedoma *et al.* [68] compared interferometric and FBG sensors at laboratory conditions with standard ECG measurements. Both signals were adequately preprocessed by filtration “ PCG signal by bandpass filter 20 ” 50 Hz and BCG signal by bandpass filter 5 ” 20 Hz. Both heart rate signals were compared to standard ECG measurement. The accuracy of heart rate detection derived from Bland-Altman statistical analysis was higher for the interferometric sensor (96.22%) than the FBG sensor (95.23%), but there was no significant difference between these methods. The authors also experimentally tested the influence of motion artifacts on the measured signals. Both optical fiber signals were relatively resistant to mild motion artifacts (gentle movements of the legs, hands, rapid breathing, coughing) compared to ECG, but not to more vigorous motion (whole body dynamic exercise, like walking). Given the similarity between these two approaches, consideration should be given to other differentiating factors, including the size of the sensor (interferometric $>$ FBG), susceptibility to acoustic interference (interferometric $>$ FBG), sensitivity of the sensor (interferometric $>$ FBG), and susceptibility to environmental influences (FBG $>$ interferometric). Moreover, the FBG analysis must be performed spectrally, thereby increasing the cost of the resulting measuring system and providing lower power and Signal-to-Noise ratio (SNR).

In an effort to simplify the patient's preparation and to overcome the motion artifacts described above, Dziuda *et al.* [74], [77], [80], placed the FBG sensor beneath the (supine) patient. They achieved satisfactory results (relative error $<6.6\%$ related to ECG) using 1.5 T MR, when preprocessing the BCG signal by 2 ” 60 Hz bandpass filter to reduce the respiratory waveform in the signal and thus to detect the heart rate more accurately. On the other hand, Nedoma *et al.* [78] implemented more sophisticated encapsulation of sensor, which provides similarly accurate measurements but increases the patient's comfort.

Nedoma *et al.* [81], also at 1.5 T, used a fiber-glass encapsulated MRI sensor, so created a sensor of minimal size and weight (2 g) when the same or even higher measurement accuracy is achieved. In this case, the sensor was placed in the pulmonary region of the chest as a part of the elastic band. The authors preprocessed the heart rate signal using bandpass filter at frequencies 2 ” 20 Hz. The mean delay in cardiac activity detection from BCG vs. ECG reached 127 ms. Based on very satisfactory results (relative error $<5\%$ related to ECG), development efforts are underway to extend this work to the 3 T environment.

The first steps in CMRI triggering using fiber-optic technology were performed in rodents with a great promise [82], [83]. In whole-body 3 T scanner, Nedoma *et al.* [84] proposed cardiac triggering using FBG sensor located on the patient's chest. According to the radiologists, the diagnostic image quality was comparable to one obtained by ECG. In the FBG-triggered images, no artifacts occured and the data was acquired in the desired cardiac phase.

G. Acoustic Methods

Due to the shortcomings of ECG measurements during MRI acquisition, research has also begun to focus on sensing cardiac activity using an acoustic signal derived from PCG (see

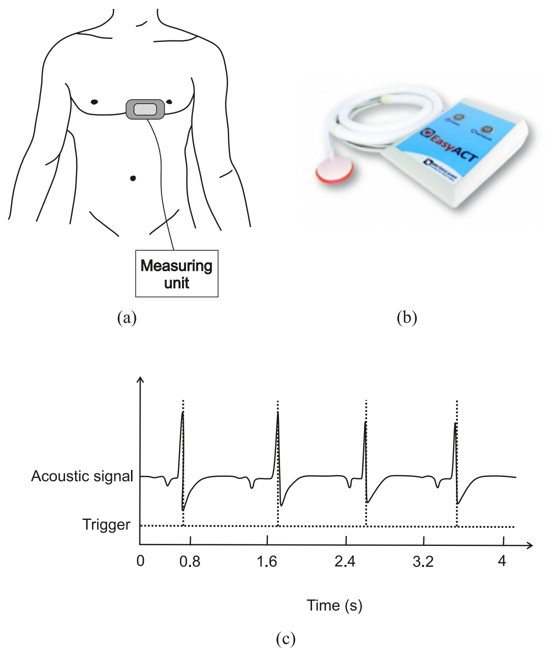

Fig. 20. Illustration of acoustic system principles and deployment: (a) Typical placement of the acoustic sensor for heart rate recording; (b) Example of acoustic sensor and measuring unit for the heart activity measurement [96]; (c) Waveform of the acoustic signal with the trigger signal.

Figure 20(c)). The PCG signal has already been used for both prospective and retrospective triggering in field strengths up to 7T [27], [28], [31], [39], [94], [95]. Remarkably, acoustic triggering is associated with less MR artifacts or other visible disturbances or magnetohydrodynamic effects across field strengths (in the range of 0.3 “ 7 T), providing high diagnostic image quality [31] with <1% mis-triggering rate [39], compared to ECG monitoring, with an error rate as high as 30% [27]. PCG monitoring has several other advantages over conventional ECG, being less ”invasive”(no need to shave the chest), and having fewer cables and sensors applied to the patient, avoiding high voltage induction potential.

The measurement is performed by an electronic stethoscope, and the first heart sound determines the trigger pulse. Although the first sound is delayed beside the R wave, a delay of about 30 ms does not affect CMRI examination by retrospective triggering [27], [28]. For extracting the first heart sound, Nassenstein *et al.* [94] use FIR Hamming low-pass filter and a thresholding algorithm based on the first sound's higher loudness (greater amplitude) in comparison with the second heart sound. Frauenrath *et al.* [31] use a covering window, which allows defining the delay with which the algorithm receives the trigger signal. Thus, the trigger is induced only once for a given period of physiological heart movement, e.g., only the first heart sound is selected using a 400 ms long delay, while rejecting the second sound.

The MRI gating acoustic sensor (see Figure 20(b)) is usually placed on the patient's chest (see Figure 20(a)) and the PCG signal is conducted through a suitable medium to the control room. The patient's anatomy significantly influences the ideal location of the sensor as the sensor must be in close contact with the chest (e.g., the left side of the sternum towards the apex). Using the elastic band can fix the sensor to prevent its moving over the patient's body during the entire examination [94].

Although the PCG signal is resistant to MR artifacts, acoustic noise due to gradient coil switching, or noise that occurs during examination along with respiratory triggering by navigation echoes (see Section III-C) can interfere [31]. Then, the signal sent through the acoustic waveguide must be appropriately filtered. Frauenrath *et al.* [39] use a second-order low-pass filter with a cut-off frequency of 150 Hz to eliminate high-frequency noise while retaining the desired PCG signal content. This approach is supplied by an RC high-pass filter to remove very low frequencies and the signal derivation in [31]. In [27], the authors preprocess a signal by 3 rd order Chebychev filter with a cut-off frequency of 105 Hz, since the predominant energy of cardiac activity lies below 100 Hz.

Signal distortion can also be prevented by using an optoacoustic sensor, where the acoustic signal is converted into an optical signal and conducted to the control unit through an optical fiber. In this way, no interaction of the measuring device with a static magnetic, gradient, or RF field occurs. Maderwald *et al.* [95] successfully tested this sensor in a 7 T magnetic field, where acoustic device synchronization was successful in both healthy subjects and arrhythmia patients. Nassenstein *et al.* [94] presented retrospective PCG triggering by an optoacoustic sensor in clinical practice (at 1.5 T) to assess left ventricular function. In a few cases (5%), PCG synchronization failed, but image quality and artifact occurrence were closely correlated with ECG triggering. In addition, the post-processing algorithm enabled successful triggering even in the case of pathological murmurs in the PCG signal.

H. Ultrasound Methods

Using an ultrasound probe in Doppler mode introduces an interesting alternative to standard ECG triggering. In this approach, an A-mode ultrasound probe (see Figure 21(b)) measures cardiac function using a 2.5 MHz, 4 MHz, or 8.1 MHz frequency, depending on the sequence used and the part of the cardiovascular system providing the triggering information [106]. Such Doppler ultrasound (DUS) recording allows the measurement of RR intervals similar to ECG or PPG and provides the image quality comparable to these types of measurements. The DUS signal contains two important points “ A wave and E wave, which represent the heart cycle. The E wave is a sign of early left ventricle relaxation (immediately following mitral valve opening), while the A wave represents flow through the mitral valve following atrial contraction. By convention, E wave detection is used to generate the synchronization signal (see Figure 21(c)) [107], [108]; although, one could argue that synchronizing to the A wave with an appropriate trigger delay would more closely align to synchronization with the QRS complex. Indeed, E wave triggering introduces a significant time delay, relative to ventricular depolarization measured by ECG. While some have tried to correct this by using prolonged trigger delays (in the range of 400 ” 600 ms), this is highly variable and

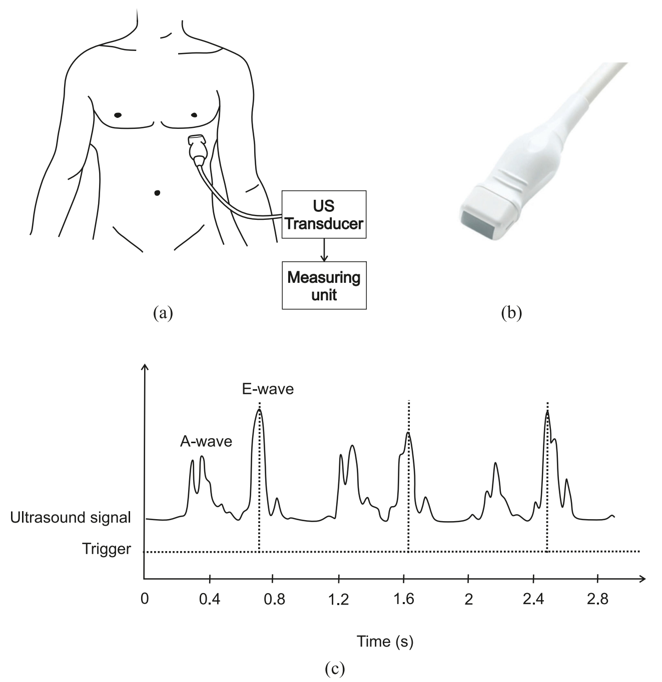

Fig. 21. Illustration of Doppler ultrasound system principles and deployment: (a) Principle of Doppler ultrasound measurement for heart activity recording, (b) Example of ultrasound probe for heart activity measurement [109], (c) Doppler ultrasound waveform with its trigger signal.

not entirely predictable [107]. However, studies did not confirm a significant difference from ECG triggering and the measured parameters showed comparable results at 1.5 T. This triggering method has indeed been validated at MR field strengths up to 3 T, see [106]–[108], with great promise even at higher field strengths due to low impressibility of DUS signal by a magnetic field. However, the limitation of this method lies in the motion artifacts of the probe placed on the patient's body and also in the inaccuracy of E-wave detection (or A wave detection) in the case of some disorders, such as mitral valve insufficiency, myocardial infarction, or tachycardia [108].

A modified, commercially available cardiotocograph (CTG) can be used to record cardiac activity during retrospective gating of CMRI by the DUS method. The CTG is housed outside the scan room, connected to the ultrasound probe, which is positioned on the chest of the patient, in the apical position (Figure 21(a)). The probe transmits a signal at a frequency of 1024 MHz with a repetition rate of 3.2 kHz, which is further processed by CTG and filtered to obtain an envelope ranged at 0 " 10 Hz. Notably, compared to conventional ECG gating, the DUS method achieves comparable results in image quality, time variability of the synchronization signal, and other monitored parameters (left ventricular volumetry, aortic velocimetry) [108].

I. Accelerometric Methods

Cardiac activity can also be measured by means of seismocardiography (SCG), which represents the course of vibration of the chest surface and acceleration of the thoracic wall resulting from cardiac contraction and blood ejection into blood vessels.

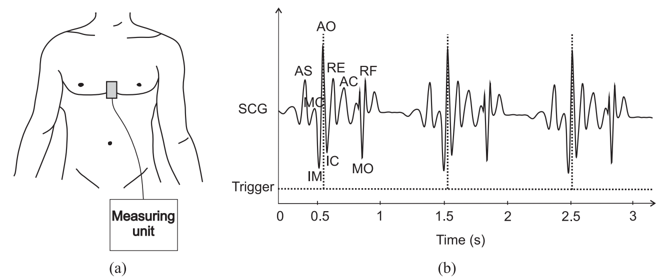

Fig. 22. Illustration of accelerometric system principles and deployment: (a) Typical placement of accelerometer for cardiac activity measuring, (b) seismocardiogram with its trigger signal.

In diagnostics, this signal has the advantage of interpreting the infrasound manifestations of heart activity in the frequency range of 0–30 Hz, which the human ear may not detect during a common examination of heart sounds.

By default, an accelerometer or a gyroscope located on the sternum (see Figure 22(a)) senses the SCG signal. Still, some studies introduced its placement at the apex of the heart and at the lower-left or upper-right edge of the sternum [110]. Using a three-axis accelerometer, SCG components are present in all three axes, each representing a specific pattern. However, the dorso-ventral component is usually used for analysis [111]. Several waveforms characterize the SCG signal, and their marking represents a specific physiological event of cardiac contraction: AS " atrial systole, MC " mitral valve closure, IM " isovolumetric contraction, AO " aortic valve opening, RE " rapid ejection, AC " aortic valve closure, MO " mitral valve opening and RF " rapid filling (see Figure 22(b)).

The measurement of the SCG signal was used to detect heart rate in [112]–[117], where this method showed adequate accuracy compared to a conventional ECG approach, reaching correlation with ECG heart rate >0.99 or detection error rate $<0,6\%$. Some researches demonstrated the accuracy of heart rate determination from the SCG signal by triggering investigations in computed tomography and nuclear medicine [118], [119]. These studies achieved more accurate detection of cardiac events and hence higher image quality for diagnostic purposes than ECG approach.

Within the MRI environment, cardiac activity has been measured using a piezoelectric accelerometer [120], with good electromagnetic compatibility. No artifacts due to the magnetic environment occurred in the measured signal, and the authors considered the evaluation of wall movement abnormalities to be a good indicator of coronary ischemia, as it is more sensitive and specific compared to the ECG method. The disadvantage of the SCG sensing is its susceptibility to interference due to gradient coil pulses. However, simple filtration can eliminate this interference, e.g., using a reference accelerometer sensing only external noise. The signal is also influenced by the patient's respiratory activity, which modulates the signal, but it is not detectable within one heart cycle.

Martinek *et al.* [121] proposed an SCG triggering method in the 3 T MR environment. The authors, however, do not use a standard accelerometer as in the studies mentioned above, but

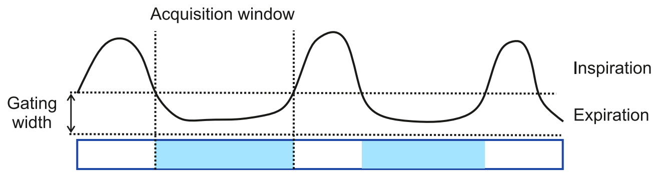

Fig. 23. Respiratory trace with principle of respiratory gating – the acquisition occurs during the rest phase of respiratory cycle.

their own sensor " plastic funnel designed and generated using a 3D printer. This sensor is placed on the patient's chest using an elastic band and senses an SCG signal in one vector perpendicular to the sensor mounting location. Then, the acoustic tube conducts the signal to the measuring microphone in the control room. This system excels in its high resistance to external sounds and vibrations. However, signal processing includes filtration in the range of 0 " 40 Hz to ensure the optimal signal quality. The filtration introduces the delay into the SCG signal, whose total value is 45 " 120 ms. Nevertheless, this delay did not affect the accuracy of acquisition triggering because the SCG triggering reached sharper image with a higher myocardium/blood contrast according to experts image assessment. Considering the objective evaluation, the quality of SCG and ECG triggered images is comparable.

III. Respiratory Gating Methods

During respiration, the organs move with the chest wall and diaphragm, changing their physical location within the bore of the scanner throughout the cardiac cycle. Because images are prescribed according to specific x, y, z coordinates, imaging is often performed during a breath-hold; designed to keep the organ of interest in the same field of view. There are many scenarios where breath-hold imaging is contraindicated. For example, many patients struggle to hold their breath beyond 10 seconds. So, depending on the imaging sequence (which can often last 1–3 minutes, and beyond), it may not be possible to acquire images during a single breath-hold. Moreover, breath-holding can be physically challenging for some individuals, limiting compliance during longer scans. To overcome these challenges, respiratory gating (see Figure 23) is often performed, whereby image acquisition is synchronized to a specific period of the respiratory cycle (usually end-expiration). Such respiratory gating also introduces new opportunities to investigate patients under general anesthesia or small children.

In the past, mechanical bellows and piezoelectric sensors were used to monitor chest movements. In current clinical practice, respiratory triggering is typically performed using navigation echoes. This method is based on the transmission of an additional radiofrequency (RF) pulse that precedes the acquisition. There are two types of navigators; first, which monitors the real-time position of the diaphragm (liver-dome scout, see Figure 25(a)) and second that detects tiny fluctuations of the main magnetic field induced by liver movement during the breathing cycle (phase scout, see Figure 25(b)) [1], [24], [122].

Respiratory gating using navigators is the most frequently used in T2 HASTE (Half-Fourier acquired single-shot turbo-spin-echo), T1 opposed phase, DWI (Diffusion-Weighted Imaging), and T2 3D hydrographic sequences, which allow a basic assessment of the abdominal organs in the native image. Figure 24 illustrates the effect of navigator gating on these abdominal imaging sequences. Note the improved boarder delineation, heightened CNR, and improved differentiation of individual structures and overall image sharpness when the respiratory gating is performed.

A. Respiratory Gating Challenges

Respiratory motion compensation is often more preferred than breath-holding method due to the previously mentioned challenges in imaging patients who are not able to hold their breath for the desired time period. Moreover, the heart border may drift during inspiration before breath-holding and then, during expiration due to the increase of heart rate toward the end of the breath-hold. It was found that the diaphragm position was irregular and unsteady or drifted continuously during breath holding in 33% of patients [123].

Generic limitations to respiratory triggering and gating arise from violation of the two basic assumptions, namely periodicity of the respiratory excursions and stationarity of the imaged object. For example, breathing may be very irregular in pediatrics, severely limiting the achievable image quality. However, motion-compensated exams also fail sporadically in adults due to breathing position drifts and changes in breathing patterns. Respiratory drift of diaphragm position outside of the acceptance window can be seen in patients who are initially anxious or fall asleep during the scanning. Another potential problem is the artifact generated by structures not moving with the region of interest. This may be reduced by applying spatial saturation bands over static structures, such as the chest wall. Besides, the hysteretic effects of the heart motion are seen between inspiration and expiration, which are being solved by development of subject-specific prospective respiratory motion models [123], [124].

As mentioned above, respiratory bellows have been traditionally used to monitor chest wall expansion. However, this technique is not consistently reliable because the temporal relationship between chest wall expansion and intraabdominal/intrathoracic organ position is not constant. On the contrary, the use of navigation echoes is more direct technique to monitor respiratory motion. The crucial issue in this approach is the placement of the navigator. When using phase scout, the navigator is located within homogeneous liver tissue (see Figure 25(d)). In contrast, liver-dome scout requires its position directly on the diaphragm with a peak of the dome of the right hemidiaphragm (see Figure 25(c)), allowing easy setup and sharp diaphragm edge. The diaphragm position is clearly delineated by the liver-lung interface on the right hemidiaphragm. Subject-specific parameters are usually determined in a low-resolution prescan by using either multiple guided breath holds or free breathing. The multiple images acquired at different respiratory positions

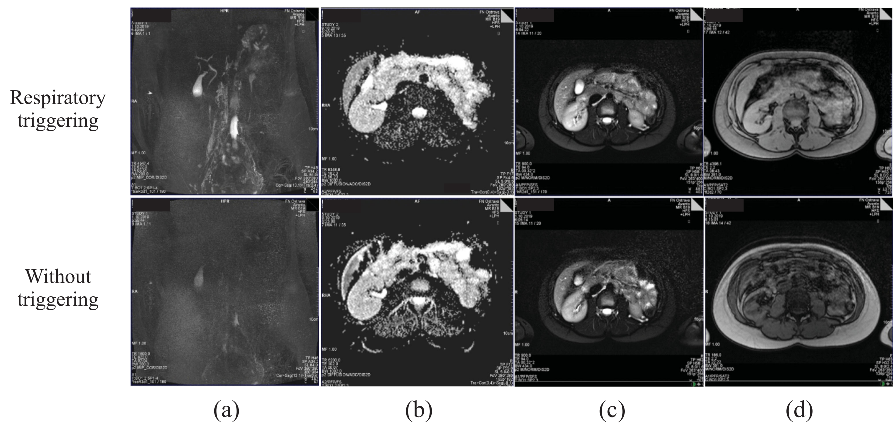

Fig. 24. Comparison of respiratory-triggered and non-triggered images using (a) T2-Weighted Hydrographic Sequence, (b) DWI Sequence, (c) T2 HASTE Sequence and (d) T1 Opposed Phase Sequence.

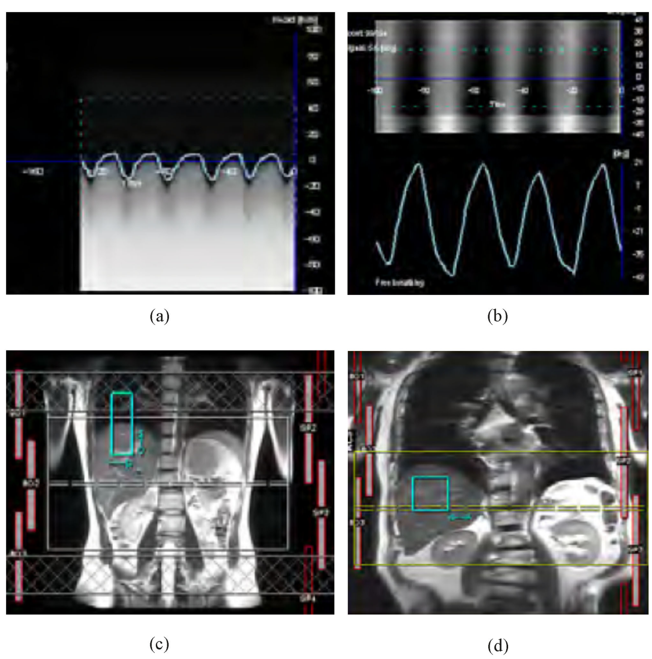

Fig. 25. Illustration of respiratory triggering system principles and deployment: (a) navigator data showing liver (gray)-lung (dark) interface with diaphragm motion, (b) navigator data showing respiratory motion from magnetic field fluctuations. Example of navigator positioning: (c) liver-dome scout image, (d) phase scout image [122].

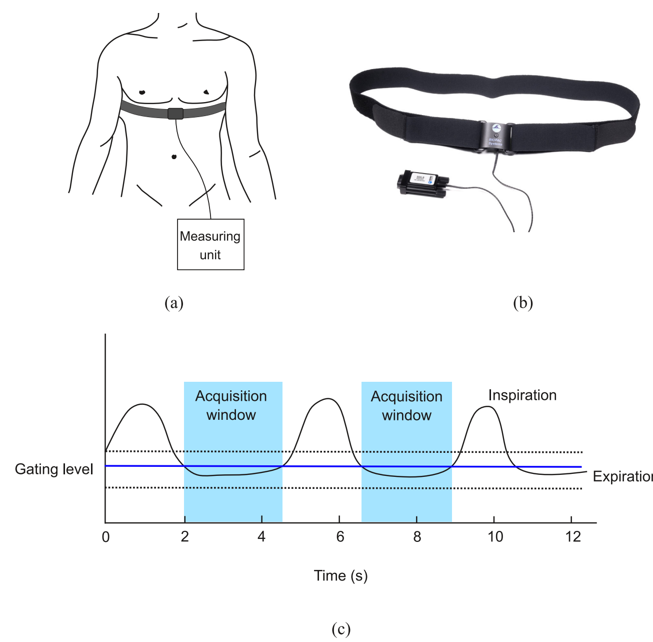

Fig. 26. Illustration of respiratory triggering system principles and deployment: (a) Typical placement of respiratory belt, (b) Example of respiratory belt [34], (c) Respiratory waveform with the localization of the synchronized acquisition window.

are registered to one image defined as a reference to determine the elements of the transformation matrix [123], [125], [126].

In addition to today's standard approaches, other respiratory triggering options have been explored, such as infrared reflectometry [127], spirometry [128], capnometry (a measurement of exhaled CO2 tension) [129], or ultrasound [130]. Today, the research focuses mainly on the optimization of navigators, S-G methods, and measurements using optical fibers.

B. Respiratory Belts

Sensing using respiratory belts, based on the function of piezoelectric sensors (see Figure 26(b)), is a standard and relatively simple way of measuring respiratory activity. The belt is placed around the patient's chest or abdomen (see Figure 26(a)) to monitor its breathing movements. According to the respiratory curve obtained by these sensors, a triggered acquisition is in the process during exhalation when the diaphragm movement is minimal (see Figure 26(c)). Since the acquisition takes place only in part of the respiratory cycle, this simple triggering by respiratory activity can extend the scanning time by 50 to 300% [20]. The main benefit of this measurement lies in a continuous signal that does not interfere with the imaging and has no effect on the MR signal (unlike navigators or S-G techniques). Also, the quality of the respiratory signal is independent of the magnetic field strength [131]. However, disadvantages include the fastening of the belt itself, which must enclose the patient's body with a certain pressure, and the susceptibility to artifacts due to the patient's movement [132].

Santelli *et al.* [131] evaluated the accuracy of triggering using respiratory sensors placed on the abdominal and thoracic areas of the patient and its impact on the quality of coronary MR images. The respiratory signal had a correlation $R = 0.9 \pm 0.05$ with the diaphragm position, but the correlation decreased when placing the belt around the chest. Not surprisingly, the respiratory triggered image was higher in quality (less motion artifact) than the non-triggered image.

Kandpal *et al.* [133] investigated the differences between the 1.5 T DWI sequence examination triggered using respiratory belts and breath-hold acquisition. Both healthy subjects and subjects with renal lesions (malignant and benign) were examined. None of the images contained motion artifacts, so image analysis and diagnosis were successful. However, a statistically significant difference between the CNR of lesions when triggering (32.9) and breath-holding (16.6) occurred. A respiratory-gated acquisition also achieved a higher SNR (44.2) than a breath-hold acquisition (28.1). However, the mean relative contrast values did not show a statistically significant difference. Oshinski *et al.* [134] conducted similar research when the subjectively assessed image quality was higher in triggering than in breath-holding as well as SNR (14.5 vs. 11.9).

In the CMRI area (1.5 T field strength), the effectiveness of triggering by respiratory bands has been investigated in [135] when assessing myocardial infarction, where patients have a major difficulty holding their breath for the required time (often longer than 20 s). While the 2D free-breathing sequence was successful in all cases, two patients failed in 3D triggered examination due to their inability to hold their breath adequately and irregular heartbeat. The image quality assessed visually achieved better results in case of 3D triggered examinations (good or excellent only) than breath-hold sequence (twice suboptimal, twice completely unsuccessful). Also, the triggered examination reached higher CNR (545 vs 327).

C. Navigation Echoes

The method of navigation echoes represents a modern approach to the respiratory triggering, see [20], [24], [131], [134], [136]–[140], and is used in clinical practice in imaging of abdominal area. Such an echo is the response of an additional RF pulse (about 20 ms long and emitted every 200 ms) that allows the MR system to detect the position of the diaphragm and thereby monitor its movement. Once the acceptance window (placed at a certain level) registers the diaphragm position, it triggers the acquisition (see Figure 27) [24].

The navigation system brings the increased comfort of the patient, who does not need to be prepared for MR examination by application of sensors. Higher accuracy of triggering using navigators than respiratory belts has been demonstrated in [131], [134], [136]. However, even if occasionally, navigation pulses can affect the MR signal itself, which decreases the image quality. Also, the navigator method is not entirely independent of magnetic field strength (at 3 T or 7 T), which can result in artifacts in the image [131].

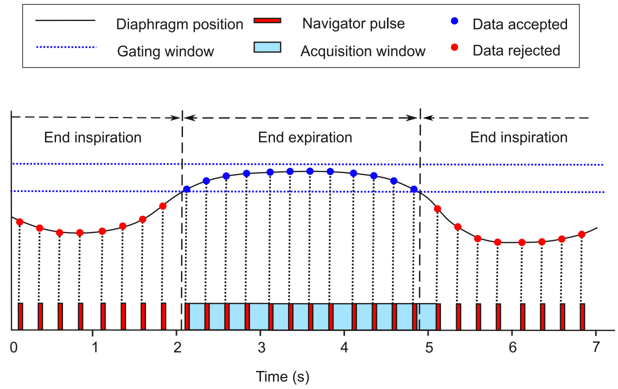

Fig. 27. The principle of navigator triggering.

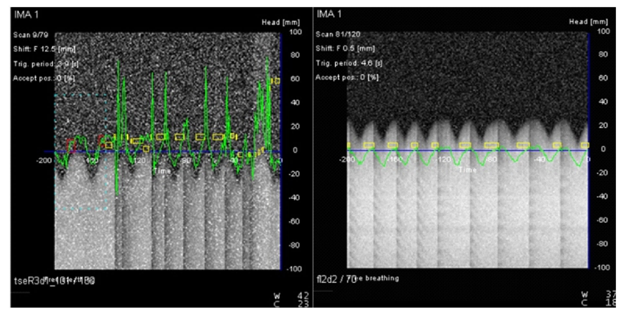

(a) (b)

Fig. 28. Diaphragm's position detection using navigators (Siemens Prisma) " the example of the (a) insufficient and (b) satisfactory breath detection.

Figure 28 illustrates an example of this respiratory monitoring approach, showing ascent and descent of the diaphragm with each breath (tracked with the green line) and image acquisition performed at end-expiration (denoted by the yellow box). Figure 28(b) shows satisfactory respiratory monitoring with regular breathing excursions, resulting in sharp and diagnostically accurate image. In contrary, degradation of the image quality can be caused by inferior respiratory recognition, when the scanner detects irregular breath waves, as in Figure 28(a).

Klessen *et al.* [137] compared the abdominal examination using navigators, and breath-hold approaches at a field strength of 1.5 T. Triggered sequences achieved higher liver-spleen contrast values (up to 131%), as well as improved visibility and sharpness of intrahepatic vessels. In [138], no significant difference between the breath-hold sequence and the triggered sequence was obtained. However, when using navigator synchronization, images were judged to be of better quality with fewer artifacts and greater sharpness. Triggered and breath-hold DWI sequences were compared in [140] at a field strength of 1.5 T, with the use of navigation echoes significantly enhancing both image quality and SNR scores (almost twice) and achieving higher kidney-lesion contrast (1.7 vs. 2.6).

Triggering by navigators in CMRI allows acquisition during a short sample window in each heart cycle (see Figure 29). The navigation echo is obtained immediately after the acquisition window, which means that a short time period elapses between the acquisition of the navigation echo and the acquisition of

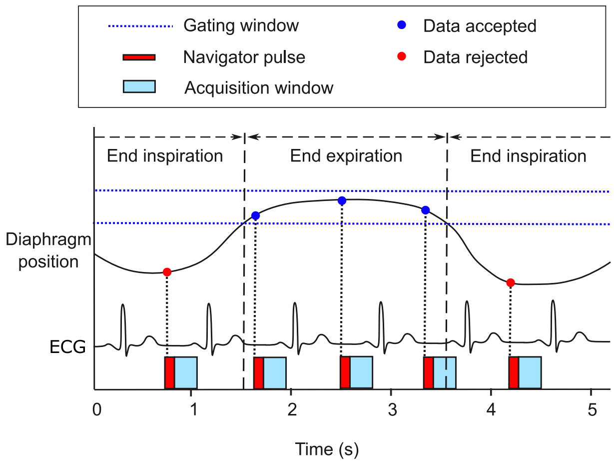

Fig. 29. The principle of navigator triggering in CMRI.

image data. However, data needs to be acquired throughout the heart cycle in CMRI, so triggering by one navigation echo within one cycle is insufficient for this purpose [141].

Peters *et al.* [139] used two navigation echoes within one heart cycle for CMRI respiratory triggering " just before the QRS complex occurred and 500 ms after that. Data is received when both navigator positions fall into the acceptance window. There was no significant difference between the image quality or the values of the observed parameters (left ventricular function and volume) by triggering and breath-holding, but the CNR of these images showed differences on behalf of the breath-hold method (47 ± 14 vs. 21 ± 10). However, the navigation echoes provided sufficient image quality for diagnosis and increased the efficiency and speed of the examination (total time for breath-holding was 10 minutes, including pauses, for triggering 3.7 minutes), which brings benefits to patients under stress or completely incapable of cooperation in breathing.

D. Self-Gating Methods

Like cardiac synchronization, S-G techniques (see Section II-E) also deal with respiratory triggering, because the afore-mentioned methods of monitoring respiratory activity may lag if the position of the chest wall changes with respect to the heart's position during several respiratory cycles. The S-G technique often allows triggering by both vital functions in CMRI examinations, where obtaining the individual signals by proper filtration (each signal has a different frequency response), see [98], [141]–[143].

The method is based on calculating the correlation between the trigger image and the target image obtained in the same heart phase and the desired position of the breath cycle. Larson *et al.* [141] filter the breath curve obtained by S-G signals and correlation using low-pass FIR filter and specify a respiratory threshold (see Figure 30), which defines the data further used to reconstruct the image at each phase of the heart cycle. This procedure increased the sharpness and contrast of the image compared to the free-breathing image without triggering, but the difference in image quality compared to the breath-hold

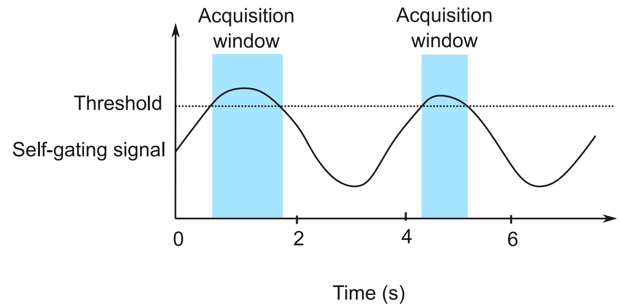

Fig. 30. Respiratory Self-Gating waveform with illustration of gating principle.

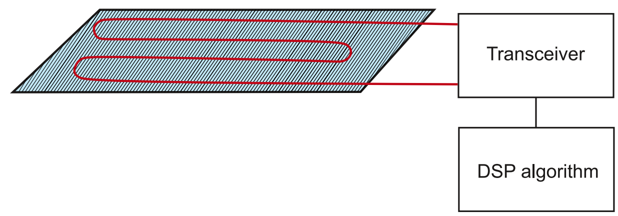

Fig. 31. Example of the micro-bend sensor implementation into mat [162].

technique was no significant, similarly to [142], [143]. Nevertheless, cardiac and respiratory S-G signals correlate strongly with externally measured signals using ECG ($R = 1.00 \pm 0$) and respiratory belts ($R = 0.82 \pm 0.1$) [143].

Other successful applications of the retrospective respiratory S-G methods were carried out in lung UTE (ultra-short echo time) imaging in [165]–[168]]. The lung investigation is particularly challenging not only because of respiratory and cardiac motion limiting the image quality, but also intrinsically low MR signal caused by the low water concentration, multiple air"tissue interfaces, or low proton density of the lung parenchyma. Since navigator sequence causes a concomitant saturation of lung parts, S-G method represents less complicated way of free-breathing lung imaging [166], [169]

Real-time S-G triggering has been demonstrated in [144], [145]. This approach promises to significantly reduce acquisition time while maintaining image quality similar to the retrospective method but requires more sophisticated software for signal detection and processing.

E. Optical Methods

The field of optical sensors and fibers also investigates the respiratory synchronization of MR, similar to the cardiac (see Section II-F), when both vital signs are often combined for the measurement of the patient's status during MRI. For measurement of breathing activity by optical sensors, researchers use interferometric sensors [61]–[66], [146]–[149], FBG sensors placed under the patient's back [70]–[73], [75], as well as micro/macro-bending fibers [90], [93], [150]–[154], which are often part of so-called smart textiles [155]–[161]. Example of the micro-bend sensor implementation into mat is shown in Figure 31. The difference in measurement of respiration compared to cardiac activity is the signal filtering in a different frequency band to maintain only the desired breath curve, i.e., within the range of 0.05–2 Hz.

Yoo *et al.* [163] presented an option of measuring only respiratory activity, which responds to changes in air temperature during inhalation and exhalation, acquired by a special sensor. The authors designed two different types of optical sensors for monitoring the respiratory rate ” nasal and abdominal. A sensor attached to the nasal cavity measures the airflow using a thermochromic pigment that changes color depending on the temperature variations within the breath cycle (inhalation/exhalation). The second type of sensor is located on the patient's abdomen and measures breathing activity as the circumference variance. The authors verified the use of the proposed sensors without deteriorating the MR image, which promises a suitability of the fiber-optic respiration sensors for respiratory monitoring during surgical procedures performed inside an MRI system.

Measurement of respiratory rate by FBG sensors in MR environment was performed in [68], [74], [77], [78], [80], [81], [164]. All these studies reached the Bland-Altman derived accuracy of the respiratory rate greater than 95% related to conventional respiratory sensors, so the optical method appears to be a good alternative to MRI respiratory triggering. In connection with heart rate monitoring, this technique becomes very interesting for MRI examinations since one sensor would be able to measure the overall vital signs of the patient, moreover continuously, as described in [83].

Fajkus *et al.* [132] tested respiratory triggering at a 3 T field strength using an FBG sensor applied to the nasal oxygen capsule. They filtered the obtained signal in the band of 0.1 ” 0.5 Hz and compared the calculated respiratory activity with the conventional measurement by respiratory belts, where the measurement by optical sensor reached an accuracy based on the Bland-Altman analysis of over 95%. According to experts, the images from both triggering methods were diagnostically beneficial, but higher contrast and sharpness of the contours were achieved when using the optical sensor. Also, according to quantitative image analysis, images triggered by FBG achieved better results than respiratory reference.

Respiratory triggering using a micro-bend sensor was tested at a field strength of 1.5 T in [162]. The optical signal reached a very high correlation $R = 0.971$ with measurements by standard respiratory sensors. No movement artifacts or blurry parts occurred in the image. The difference between the optical and navigator methods in assessing the SNR of the kidney and the CNR kidney-spleen was not significant, but the navigator method gained a significantly better diagnostic quality of the images.

IV. Discussion

The review of CMRI synchronization methods shows that today's research focuses more on the novel ones than improving the techniques most widely used in clinical practice. It is due to relatively complicated patient preparation in case of ECG/VCG and especially due to the increasing complications of high field strength examination. Also, relatively patient-friendly PPG is not suitable because of motion artifact susceptibility and long physiological delay. The contemporary research focuses on two major milestones: (1) advancement of software that can achieve adequate accuracy in the detection of synchronization points in the signal or suppress magnetic field artifacts, and (2) development of new methods of measuring vital signs that could replace standard ECG measurements in future.

Thanks to the extreme increase in computing performance in the recent years, it is possible to significantly improve the signal/image quality by using advanced processing techniques. However, relying only on software algorithms can result in a number of computer errors, which can lead to the distortion of some image segments and thus, suppress important diagnostic information. Therefore, it is undoubtedly important to pay attention to the basic entity of the entire measuring chain (sensors), which could provide a desirable accuracy already on the lowest layer and thus, together with using software algorithms, even better overall results.

Currently, acoustic and accelerometric triggering methods are most suitable to introduce into practice, providing safety and comfort for the patients and high resistance to artifacts caused by magnetic fields; efficiency of acoustic sensors has already been successfully tested at 7 T. The only drawback is susceptibility of the PCG and SCG to interference caused by gradient coil switching, and accordingly, the delay in signal transmission to the MR unit due to filtration. Other investigations, which are still in their infancy, such as optical or DUS measurements, show high-quality heart rate calculations, but some limitations have not yet proven their usability in medical practice: the optical method requires a very expensive evaluation unit, which could become more accessible over time, and inaccuracy in DUS measurements of patients with cardiac disorders means a major complication in cardiac examinations.

The research methods have several common disadvantages:

- *Non-standardized sensor placement* in contrast with ECG or VCG. The sensor location highly depends on the specific patient and his body structure; some signals show very different waveforms when placed at diverse points of the chest (e.g. SCG). Therefore, research should handle the possibilities of measurement without the complicated attachment of the sensor to the patient's body, such as sensors implemented in textiles or mats.
- *Signal delay compared to ECG signal* which is given by several attributes: (1) a physiological delay between the R wave and the alternative trigger point (first heart sound, J-wave etc., see Figure 32), and (2) other delays superimposed caused by the transmission medium, electronics ensuring signal state and conversion to a digital signal, or filtration used to remove undesirable components. Such a delayed trigger signal may lag behind the ECG trigger for hundreds of milliseconds, collecting data from the wrong phase of the cardiac cycle. Therefore, the image may lose its diagnostic value, and the acquisition needs to be repeated, extending the examination time. Thus, suppression of the signal delay in some way, such as software customization of triggering, should be used.

TABLE I
THE CLASSIFICATION OF THE PRESENTED SYNCHRONIZATION METHODS

	Type	Accuracy	Resistance	Complexity	Limitations
ECG	Cardiac	High	Low	Medium	Measures against high voltages
VCG	Cardiac	High	Medium	Medium	Measures against high voltages
Pulse Wave	Cardiac	Low	High	Low	Motion artifacts, long physiological delay
Acoustic	Cardiac	High	Medium	Medium	Long delay due to conduction and processing
Accelerometry	Cardiac	High	Medium	Low	Long delay due to conduction and processing
Optic	Cardiac, respiratory	High	High	High	Long physiological delay of FBG sensors
Doppler Ultrasound	Cardiac, respiratory	Medium	High	High	Long delay, difficult contact with the patient, heart abnormalities
Self-Gating	Cardiac, respiratory	Medium	High	High	Mild myocardial contractions, high heart rate, prospective triggering
Navigation Echoes	Respiratory	Medium	Medium	Medium	Short impulse in one heart cycle
Respiratory Belts	Respiratory	Medium	High	Low	Motion artifacts, correct positioning

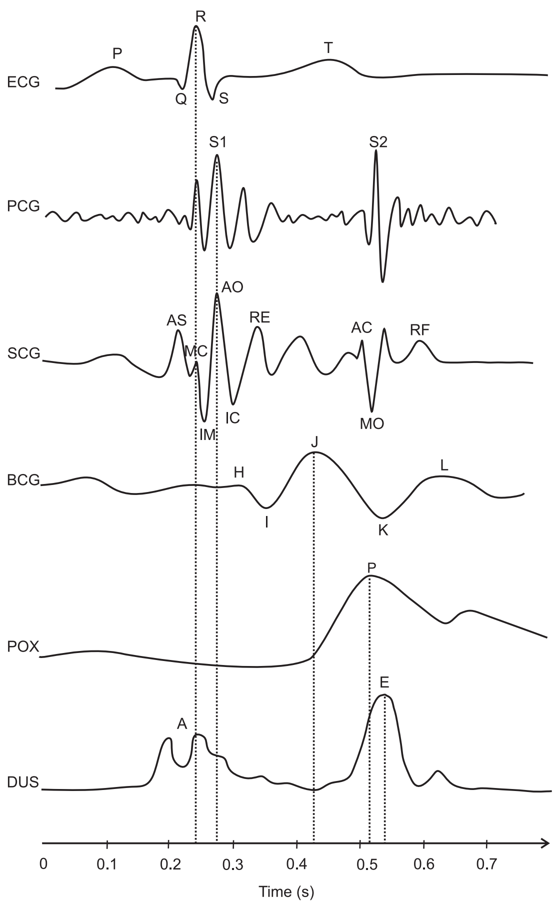

Fig. 32. Physiological delay of the individual heart signals compared to the ECG with marked peaks (trigger).

The presented S-G methods could solve the problems of sensor placement and signal delay versus ECG. Another advantage of S-G methods is the possibility of respiratory and cardiac gating altogether. Although this *double* triggering prolongs the required scan time significantly, the total examination time is shortened in cooperating patients. In case of patients unable to assist in breathing, respiratory synchronization is a necessity for a successful examination. Because respiratory compensation using navigation echoes lags due to the very small acquisition window triggered by only one navigation echo per heart cycle, a single breath-hold examination still prevails, which can cause problems for many patients.

However, shortcomings of S-G techniques lie in the realization of synchronization itself. In general, these methods have low hardware requirements at the expense of the complexity of software, which processes MR data to generate a trigger signal. Therefore, methods of measuring vital functions, which enable to distinguish a respiratory function from the heart signal by appropriate filtration (BCG, SCG), become preferred. Considering the unavailability of optical methods, acoustic and SCG methods are currently considered as most promising methods for combining cardiac and respiratory synchronization and should remain to be the subject of further research in this area.

Table I subjectively summarizes methods for cardiac and respiratory MRI synchronization with the classification of their accuracy and artifact resistance:

- *Accuracy* refers to the success of correct detection of cardiac function with sequence initiation in the desired phase of the heart/respiratory cycle, which enhances image quality. It is evaluated with respect to cases of some abnormalities (e.g., disease, arrhythmia) or technical limitations, not to the origin of MR artifacts. Accuracy is classified as follows:
  - *High*” method provides very accurate heart/respiratory phase detection and is minimally affected by abnormalities, patient’s physiology or movements.
  - *Medium* ” method provides accuracy suitable for MR gating but is limited by some of the above-mentioned problems.
  - *Low* ” method is not recommended for MR gating due to large range of limitations.

  Resistance to MR artifacts indicates the resistance to effects of the MR environment on a given signal (influence of electromagnetic field, magnetohydrodynamic effect or acoustic disturbance) and degree of independence from magnetic field strength, classified as:
  - *High* ” method is completely resistant to MR artifacts and independent from magnetic field strength.
  - *Medium*” method is affected only by one of the above-mentioned MR influences.
  - *Low* ” method is susceptible to all effects of the MR environment.

  Complexity includes computational requirements, availability, and the price of sensors or measuring unit. Computational cost is a crucial factor in implementation of the measuring system since it determines a function of the system in real-time. Price is also a key point of method feasibility for clinical practice. A method eligible for introducing into practice should accomplish a compromise between its complexity and performance/accuracy.

Specific limitations closely relate to the previous parameters but include detailed knowledge of the disadvantages of each method, which must be eliminated or reduced as best as possible in order to introduce the method into practice successfully.

V. Conclusion

Synchronization of the cardiac cycle and respiratory excursions is necessary for cardiovascular and abdominal MRI for optimal representation and image quality. The paper summarizes techniques currently available and/or under development that focus on increasing problems with measurement in high magnetic fields, nowadays reaching up to 7 T. With an extreme increase in computing performance in recent years, software-based methods, such as S-G and navigators, are the center of attention, and they underwent a huge expansion. However, they still have some disadvantages (computer errors, disturbing steady-state), which could be solved using the hardware-assisted methods based on the non-electrical measurements. From such these techniques, acoustic and accelerometric ones are the most promising not only due to the high accuracy but also thanks to their low price and easy implementation. Moreover, they would provide the possibility of monitoring the respiratory signal together with cardiac function and thus, would enable a "double" MR triggering approach, important in cardiovascular examinations, especially in non-cooperating patients. With this foundation in place, the future of MR synchronization is encouraging; however, more work is needed in order to maximize the technology available and develop new approaches not yet imagined.

References

[1] N. C. Gourtsoyiannis, Ed., *Clinical MRI of the Abdomen*. Berlin, Heidelberg: Springer Berlin Heidelberg, 2011.

[2] A. Varghese and D. J. Pennell, Eds., *Cardiovascular Magnetic Resonance Made Easy*. Edinburgh, U.K.: Churchill Livingstone, 2008.

[3] A. Stadler, W. Schima, A. Ba-Ssalamah, J. Kettenbach, and E. Eisenhuber, "Artifacts in body MR imaging: Their appearance and how to eliminate them," *Eur. Radiol.*, vol. 17, no. 5, pp. 1242–1255, Apr. 2007.

[4] R. C. Semelka, M. A. Brown, E. Altun, and R. C. Semelka, *Abdominal-Pelvic MRI*, 4th ed. Hoboken, NJ, USA: Wiley, 2016.

[5] G. Constantine, K. Shan, S. D. Flamm, and M. U. Sivananthan, "Role of MRI in clinical cardiology," *Lancet*, vol. 363, no. 9427, pp. 2162–2171, 2004.

[6] T. Sato *et al.*, "Validation study on the accuracy of echocardiographic measurements of right ventricular systolic function in pulmonary hypertension," *J. Amer. Soc. Echocardiogr.*, vol. 25, no. 3, pp. 280–286, 2012.

[7] P. C. Yang *et al.*, "New real-time interactive cardiac magnetic resonance imaging system complements echocardiography," *J. Amer. College Cardiol.*, vol. 32, no. 7, pp. 2049–2056, 1998.

[8] T. Niendorf, D. K. Sodickson, G. A. Krombach, and J. Schulz-Menger, "Toward cardiovascular MRI at 7 T: Clinical needs, technical solutions and research promises," *Eur. Radiol.*, vol. 20, no. 12, pp. 2806–2816, 2010.

[9] G. Pons-Llado and F. Carreras, *Atlas of Practical Applications of Cardiovascular Magnetic Resonance*. New York, NY, USA: Springer Science Business Media, 2005.

[10] R. R. Edelman, H. P. Mattle, D. J. Atkinson, and H. M. Hoogewoud, "MR angiography," *Amer. J. Roentgenol.*, vol. 154, no. 5, pp. 937–946, 1990.

[11] V. M. Ferreira, S. K. Piechnik, M. D. Robson, S. Neubauer, and T. D. Karamitsos, "Myocardial tissue characterization by magnetic resonance imaging," *J. Thoracic Imag.*, vol. 29, no. 3, pp. 147–154, 2014.

[12] M. Jerosch-Herold, O. Muehling, and N. Wilke, "MRI of myocardial perfusion," *Seminars Ultrasound, CT MRI*, vol. 27, no. 1, pp. 2–10, 2006.

[13] M. Schär, S. Kozerke, S. E. Fischer, and P. Boesiger, "Cardiac SSFP imaging at 3 tesla," *Magn. Reson. Med.*, vol. 51, no. 4, pp. 799–806, 2004.

[14] H. J. Michaely *et al.*, "Analysis of cardiac function comparison between 1.5 Tesla and 3.0 Tesla cardiac cine magnetic resonance imaging," *Invest. Radiol.*, vol. 41, no. 2, pp. 133–140, 2006.

[15] R. Nezafat, M. Stuber, R. Ouwerkerk, A. M. Gharib, M. Y. Desai, and R. I. Pettigrew, "B1-insensitiveT2 preparation for improved coronary magnetic resonance angiography at 3 T," *Magn. Reson. Med.*, vol. 55, no. 4, pp. 858–864, 2006.

[16] A. N. Priest, P. M. Bansmann, M. G. Kaul, A. Stork, and G. Adam, "Magnetic resonance imaging of the coronary vessel wall at 3 T. using an obliquely oriented reinversion slab with adiabatic pulses," *Magn. Reson. Med.*, vol. 54, no. 5, pp. 1115–1122, 2005.

[17] M. E. Ladd *et al.*, "Pros and cons of ultra-high-field MRI/MRS for human application," *Prog. Nucl. Magn. Reson. Spectrosc.*, vol. 109, no. 14, pp. 1–50, 2018.

[18] A. M. Gharib, A. Elagha, and R. I. Pettigrew, "Cardiac magnetic resonance at high field: Promises and problems," *Curr. Problems Diagn. Radiol.*, vol. 37, no. 2, pp. 49–56, 2008.

[19] F. von Knobelsdorff-Brenkenhoff *et al.*, "Cardiac chamber quantification using magnetic resonance imaging at 7 tesla-a pilot study," *Eur. Radiol.*, vol. 20, no. 12, pp. 2844–2852, 2010.

[20] A. D. Elster, "Questions and answers in MRI," 2021. [Online]. Available: https://mriquestions.com/motion-related-artifacts.html

[21] M. S. Nacif, A. Zavodni, N. Kawel, E.-Y. Choi, J. A. C. Lima, and D. A. Bluemke, "Cardiac magnetic resonance imaging and its electrocardiographs (ECG): Tips and tricks," *Int. J. Cardiovasc. Imag.*, vol. 28, no. 6, pp. 1465–1475, 2012.

[22] R. Y. Kwong, M. Jerosch-Herold, and B. Heydari, Eds., *Cardiovascular Magnetic Resonance Imaging*, 2nd ed., New York, NY, USA: Springer New York, 2019.

[23] R. B. van Heeswijk, G. Bonanno, S. Coppo, A. Coristine, T. Kober, and M. Stuber, "Motion compensation strategies in magnetic resonance imaging," *Crit. Rev. Biomed. Eng.*, vol. 40, no. 2, pp. 99–119, 2012.

[24] R. George, J. Dela Cruz, R. Singh, and R. Ilangovan, "MRI Master" 2021. [Online]. Available: https://mrimaster.com/index-3.html

[25] G. M. Pohost and K. S. Nayak, *Handbook of Cardiovascular Magnetic Resonance Imaging*, 2nd ed., New York, NY, USA: Informa Healthcare, c2007.

[26] S. E. Fischer, S. A. Wickline, and C. H. Lorenz, "Novel real-time r-wave detection algorithm based on the vectorcardiogram for accurate gated magnetic resonance acquisitions," *Magn. Reson. Med.: Official J. Int. Soc. Magn. Reson. Med.*, vol. 42, no. 2, pp. 361–370, 1999.

[27] T. Frauenrath *et al.*, "Acoustic cardiac triggering: A practical solution for synchronization and gating of cardiovascular magnetic resonance at 7 tesla," *J. Cardiovasc. Magn. Reson.*, vol. 12, no. 1, pp. 1–14, 2010.

[28] M. Becker *et al.*, "Comparison of left ventricular function assessment using phonocardiogram- and electrocardiogram-triggered 2D SSFP CINE MR imaging at 1.5 T. and 3.0 T," *Eur. Radiol.*, vol. 20, no. 6, pp. 1344–1355, 2010.

[29] H. Kugel *et al.*, "Hazardous situation in the MR bore: Induction in ECG leads causes fire," *Eur. Radiol.*, vol. 13, no. 4, pp. 690–694, 2003.

[30] S. A. Lange and Q. N. Nguyen, "Cables and electrodes can burn patients during MRI," *Nursing 2006*, vol. 36, no. 11, pp. 11–18, 2006.

[31] T. Frauenrath, T. Niendorf, and M. Kob, "Acoustic method for synchronization of magnetic resonance imaging (MRI)," *Acta Acustica United Acustica*, vol. 94, no. 1, pp. 148–155, 2008.

[32] The Mammendorfer Institut Für Physik Und Medizin, "MIPM: MRI-compatible products," 2021. [Online]. Available: https://www.mipm.com/en/our-products/accessories

[33] "MiRTLE Medical, LLC," MiRTLE," 2016-2017. [Online]. Available: http://www.mirtlemed.com/product.html

[34] BIOPAC Systems Inc., "BIOPAC Systems Inc.," 2021. [Online]. Available: https://www.biopac.com/product/

[35] J. W. Krug, G. Rose, D. Stucht, G. Clifford, and J. Oster, "Limitations of VCG based gating methods in ultra high field cardiac MRI," *J. Cardiovasc. Magn. Reson.*, vol. 15, no. S1, pp. 1–2, 2013.

[36] C. J. Snyder *et al.*, "Initial results of cardiac imaging at 7 tesla," *Magn. Reson. Med.*, vol. 61, no. 3, pp. 517–524, 2009.

[37] D. Abi-Abdallah, V. Robin, A. Drochon, and O. Fokapu, "Alterations in human ECG due to the MagnetoHydroDynamic effect: A method for accurate R peak detection in the presence of high MHD artifacts," in *Proc. 29th Annu. Int. Conf. IEEE Eng. Med. Biol. Soc.*, 2007, pp. 1842–1845.

[38] B. Sievers, M. Wiesner, N. Kiria, U. Speiser, S. Schoen, and R. H. Strasser, "Influence of the trigger technique on ventricular function measurements using 3-Tesla magnetic resonance imaging: Comparison of ECG versus pulse wave triggering," *Acta Radiologica*, vol. 52, no. 4, pp. 385–392, 2011.

[39] T. Frauenrath, S. Kozerke, P. Boesiger, and T. Niendorf, "Cardiac gating free of interference with electro-magnetic fields at 1.5T., 3.0T. and 7.0T," in *Proc. Annu. Meeting Int. Soc. Magn. Reson. Med.*, 2008, p. 207.

[40] F. Odille, C. Pasquier, R. Abacherli, P.-A. Vuissoz, G. P. Zientara, and J. Felblinger, "Noise cancellation signal processing method and computer system for improved real-time electrocardiogram artifact correction during MRI data acquisition," *IEEE Trans. Biomed. Eng.*, vol. 54, no. 4, pp. 630–640, Apr. 2007.

[41] J. Oster, O. Pietquin, R. Abacherli, M. Kraemer, and J. Felblinger, "Independent component analysis-based artefact reduction: Application to the electrocardiogram for improved magnetic resonance imaging triggering," *Physiol. Meas.*, vol. 30, no. 12, pp. 1381–1397, 2009.

[42] J. W. Krug, G. Rose, G. D. Clifford, and J. Oster, "ECG-based gating in ultra high field cardiovascular magnetic resonance using an independent component analysis approach," *J. Cardiovasc. Magn. Reson.*, vol. 15, no. 1, pp. 1–13, 2013.

[43] J. Oster, O. Pietquin, M. Kraemer, and J. Felblinger, "Nonlinear Bayesian filtering for denoising of electrocardiograms acquired in a magnetic resonance environment," *IEEE Trans. Biomed. Eng.*, vol. 57, no. 7, pp. 1628–1638, Jul. 2010.

[44] D. Abi-Abdallah, E. Chauvet, L. Bouchet-Fakri, A. Bataillard, A. Briguet, and O. Fokapu, "Reference signal extraction from corrupted ECG using wavelet decomposition for MRI sequence triggering: Application to small animals," *Biomed. Eng. Online*, vol. 5, no. 1, pp. 1–12, 2006.

[45] D. Abi-Abdallah, A. Drochon, V. Robin, and O. Fokapu, "Cardiac and respiratory MRI gating using combined wavelet sub-band decomposition and adaptive filtering," *Ann. Biomed. Eng.*, vol. 35, no. 5, pp. 733–743, 2007.

[46] M. Schmidt, J. W. Krug, A. Gierstorfer, and G. Rose, "A real-time QRS detector based on higher-order statistics for ECG gated cardiac," *Comput. Cardiol. 2014*, vol. 2014, no. 41, pp. 733–736, 2014.

[47] D. Stäb, J. Roessler, K. O'Brien, C. Hamilton-Craig, and M. Barth, "ECG triggering ultra-high field cardiovascular MRI," *Tomography*, vol. 2, no. 3, pp. 167–174, 2016.

[48] L. Edenbrandt, A. Houston, and P. W. Macfarlane, "Vectorcardiograms synthesized from 12-lead ECGs: A. new method applied in 1792 healthy children," *Pediatr. Cardiol.*, vol. 15, no. 1, pp. 21–26, 1994.

[49] M. Lingman *et al.*, "Transient repolarization alterations dominate the initial phase of an acute anterior infarction - a vectorcardiography study," *J. Electrocardiol.*, vol. 47, no. 4, pp. 478–485, 2014.

[50] M. Sederholm, "The origin of monitoring of acute myocardial infarction with continuous vectorcardiography," *J. Electrocardiol.*, vol. 47, no. 4, pp. 418–424, 2014.

[51] D. Cortez, J. M. Bos, and M. J. Ackerman, "Vectorcardiography identifies patients with electrocardiographically concealed long QT syndrome," *Heart Rhythm*, vol. 14, no. 6, pp. 894–899, 2017.

[52] J. M. Chia, S. E. Fischer, S. A. Wickline, and C. H. Lorenz, "Performance of QRS detection for cardiac magnetic resonance imaging with a novel vectorcardiographic triggering method," *J. Magn. Reson. Imag.*, vol. 12, no. 5, pp. 678–688, 2000.

[53] N. Spicher, M. Kukuk, S. Maderwald, and M. E. Ladd, "Initial evaluation of prospective cardiac triggering using photoplethysmography signals recorded with a video camera compared to pulse oximetry and electrocardiography at 7T. MRI," *Biomed. Eng. Online*, vol. 15, no. 1, pp. 1–28, 2016.

[54] N. Spicher, S. Maderwald, M. E. Ladd, and M. Kukuk, "Heart rate monitoring in ultra-high-field MRI using frequency information obtained from video signals of the human skin compared to electrocardiography and pulse oximetry," *Curr. Directions Biomed. Eng.*, vol. 1, no. 1, pp. 69–72, Sep. 2015.

[55] J. Hodel *et al.*, "Intracranial cerebrospinal fluid spaces imaging using a pulse-triggered three-dimensional turbo spin echo MR sequence with variable flip-angle distribution," *Eur. Radiol.*, vol. 21, no. 2, pp. 402–410, 2011.

[56] J. W. Berthold, "Historical review of microbend fiber-optic sensors," *J. Lightw. Technol.*, vol. 13, no. 7, pp. 1193–1199, Jul. 1995.

[57] Y. Wang *et al.*, "Intensity measurement bend sensors based on periodically tapered soft glass fibers," *Opt. Lett.*, vol. 36, no. 4, pp. 558–560, 2011.

[58] P. Samartkit and S. Pullteap, "Fiber optic sensor applications for vital signs monitoring: A review," in *Proc. 7th Int. Elect. Eng. Congr.*, 2019, pp. 1–4.

[59] L.-G. Durand and P. Pibarot, "Digital signal processing of the phonocardiogram: Review of the most recent advancements," *Crit. Rev. Biomed. Eng.*, vol. 23, no. 3/4, pp. 163–219, 1995.

[60] C. Will, K. Shi, F. Lurz, R. Weigel, and A. Koelpin, "Intelligent signal processing routine for instantaneous heart rate detection using a six-port microwave interferometer," in *Proc. Int. Symp. Intell. Signal Process. Commun. Syst.*, 2015, pp. 483–487.

[61] P. Podbreznik, D. Donlagic, D. Lesnik, B. Cigale, and D. Zazula, "Cost-efficient speckle interferometry with plastic optical fiber for unobtrusive monitoring of human vital signs," *J. Biomed. Opt.*, vol. 18, no. 10, pp. 1–8, Oct. 2013.

[62] S. Sprager, D. Donlagic, and D. Zazula, "Monitoring of basic human vital functions using optical interferometer," in *Proc. IEEE 10th Int. Conf. Signal Process.*, 2010, pp. 1–4.

[63] S. Sprager, D. Donlagic, and D. Zazula, "Estimation of heart rate, respiratory rate and motion by using optical interferometer as body sensor," in *Proc. Signal Image Process.*, 2011, pp. 280–287.

[64] S. Šprager, A. Holobar, and D. Zazula, "Feasibility study of heartbeat detection from optical interferometric signal by using convolution kernel compensation," in *Proc. Int. Conf. Bio-Inspired Syst. Signal Process.*, 2013, pp. 396–400.

[65] I. Cikajlo, C. S. Š. T. D. Z. Erjaveca, and D. Šprager, "Cardiac arrhythmia alarm from optical interferometric signals during resting or sleeping for early intervention," *Biocybern. Biomed. Eng.*, vol. 36, no. 1, pp. 267–275, 2016.

[66] D. Zazula and S. Sprager, "Detection of the first heart sound using fibre-optic interferometric measurements and neural networks," in *Proc. 11th Symp. Neural Netw. Appl. Elect. Eng.*, 2012, pp. 171–176.

[67] Y.-H. Hsieh and N.-K. Chen, "Micro tapered Mach–Zehnder fiber interferometer for monitoring pressure fluctuation and its applications in pulse rate detection," in *Proc. 6th IEEE/Int. Conf. Adv. Infocomm Technol.*, 2013, pp. 113–115.

[68] J. Nedoma *et al.*, "Magnetic resonance imaging compatible non-invasive fibre-optic sensors based on the bragg gratings and interferometers in the application of monitoring heart and respiration rate of the human body: A comparative study," *Sensors*, vol. 18, no. 11, pp. 1–30, 2018.

[69] P. Roriz, L. Carvalho, O. Frazão, J. Santos, and J. Simões, "From conventional sensors tofibre optic sensors for strain and forcemeasurements in biomechanics applications: A review," *J. Biomech.*, vol. 47, no. 6, pp. 1251–1261, 2014.

[70] Ł. Dziuda, "Fiber-optic sensors for monitoring patient physiological parameters: A review of applicable technologies and relevance to use during magnetic resonance imaging procedures," *J. Biomed. Opt.*, vol. 20, no. 1, pp. 1–23, 2015.

[71] K. Chethana, A. S. G. Prasad, S. N. Omkar, and S. Asokan, "Fiber bragg grating sensor based device for simultaneous measurement of respiratory and cardiac activities," *J. Biophoton.*, vol. 10, no. 2, pp. 278–285, 2017.

[72] L. Dziuda, F. W. Skibniewski, M. Krej, and J. Lewandowski, "Monitoring respiration and cardiac activity using fiber bragg grating-based sensor," *IEEE Trans. Biomed. Eng.*, vol. 59, no. 7, pp. 1934–1942, Jul. 2012.

[73] M. Fajkus, J. Nedoma, R. Martinek, V. Vasinek, H. Nazeran, and P. Siska, "A non-invasive multichannel hybrid fiber-optic sensor system for vital sign monitoring," *Sensors*, vol. 17, no. 12, pp. 1–17, 2017.

[74] Ł. Dziuda, F. W. Skibniewski, M. Krej, and P. M. Baran, "Fiber Bragg grating-based sensor for monitoring respiration and heart activity during magnetic resonance imaging examinations," *J. Biomed. Opt.*, vol. 18, no. 5, pp. 278–285, 2013.

[75] D. Lo Presti *et al.*, "Wearable system based on flexible FBG for respiratory and cardiac monitoring," *IEEE Sensors J.*, vol. 19, no. 17, pp. 7391–7398, Sep. 2019.

[76] Y. Haseda, J. Bonefacino, H. -Y. Tam, S. Chino, S. Koyama, and H. Ishizawa, "Measurement of pulse wave signals and blood pressure by a plastic optical fiber FBG sensor," *Sensors*, vol. 19, no. 23, pp. 1–11, 2019.

[77] L. Dziuda, M. Krej, and F. W. Skibniewski, "Fiber Bragg grating strain sensor incorporated to monitor patient vital signs during MRI," *IEEE Sensors J.*, vol. 13, no. 12, pp. 4986–4991, Dec. 2013.

[78] J. Nedoma *et al.*, "Validation of a novel fiber-optic sensor system for monitoring cardiorespiratory activities during MRI examinations," *Adv. Elect. Electron. Eng.*, vol. 15, no. 3, pp. 536–543, 2017.

[79] Ł. Dziuda and F. W. Skibniewski, "A new approach to ballistocardiographic measurements using fibre bragg grating-based sensors," *Biocybern. Biomed. Eng.*, vol. 34, no. 2, pp. 101–116, 2014.

[80] L. Dziuda, J. Lewandowski, F. Skibniewski, and G. Nowicki, "Fibre-optic sensor for respiration and heart rate monitoring in the MRI environment," *Procedia Eng.*, vol. 47, pp. 1291–1294, 2012.

[81] J. Nedoma, M. Fajkus, R. Martinek, and H. Nazeran, "Vital sign monitoring and cardiac triggering at 1.5 tesla: A practical solution by an MR-Ballistocardiography fiber-optic sensor," *Sensors*, vol. 19, no. 3, pp. 1–22, 2019.

[82] A. C. S. Brau, C. T. Wheeler, L. W. Hedlund, and G. A. Johnson, "Fiber-optic stethoscope: A cardiac monitoring and gating system for magnetic resonance microscopy," *Magn. Reson. Med.*, vol. 47, no. 2, pp. 314–321, 2002.

[83] A. Rengle, L. Baboi, H. Saint-Jalmes, R. Sablong, and O. Beuf, "Optical cardiac and respiratory device for synchronized MRI on small animal," in *Proc. 29th Annu. Int. Conf. IEEE Eng. Med. Biol. Soc.*, 2007, pp. 2046–2049.

[84] J. Nedoma *et al.*, "A novel FBG-Based triggering system for cardiac MR imaging at 3 tesla: A pilot pre-clinical study," *IEEE Access*, vol. 8, pp. 181205–181223, 2020.

[85] J. De Jonckheere *et al.*, "OFSETH: Optical fibre embedded into technical textile for healthcare, an efficient way to monitor patient under magnetic resonance imaging," in *Proc. 29th Annu. Int. Conf. IEEE Eng. Med. Biol. Soc.*, 2007, pp. 3950–3953.

[86] Z. Chen, J. T. Teo, S. H. Ng, and X. Yang, "Portable fiber optic ballistocardiogram sensor for home use," *Proc. SPIE*, vol. 8218, 2012, Art. no. 82180X.

[87] Z. Chen, I. Gannot, J. T. Teo, S. H. Ng, and H. Yim, "Smart pillow for heart-rate monitoring using a fiber optic sensor," in *Proc. SPIE*, vol. 7894, 2011, Art. no. 789402.

[88] K. Krebber *et al.*, "Smart technical textiles based on fibre optic sensors," *Proc. SPIE*, vol. 8421, 2012, Art. no. 84212.

[89] A. Grillet *et al.*, "Optical fiber sensors embedded into medical textiles for healthcare monitoring," *IEEE Sensors J.*, vol. 8, no. 7, pp. 1215–1222, Jul. 2008.

[90] X. Yang *et al.*, "Textile fiber optic microbend sensor used for heartbeat and respiration monitoring," *IEEE Sensors J.*, vol. 15, no. 2, pp. 757–761, Feb. 2015.

[91] D. Lo Presti *et al.*, "Cardio-respiratory monitoring in archery using a smart textile based on flexible fiber Bragg grating sensors," *Sensors*, vol. 19, no. 16, pp. 1–14, 2019.

[92] D. L. Presti *et al.*, "Cardiac monitoring with a smart textile based on polymer-encapsulated FBG: Influence of sensor positioning," in *Proc. IEEE Int. Symp. Med. Meas. Appl.*, 2019, pp. 1–6.

[93] Z. Chen, D. Lau, J. T. Teo, S. H. Ng, X. Yang, and P. L. Kei, "Simultaneous measurement of breathing rate and heart rate using a microbend multimode fiber optic sensor," *J. Biomed. Opt.*, vol. 19, no. 5, pp. 1–11, 2014.

[94] K. Nassenstein *et al.*, "Cardiac MRI: Evaluation of phonocardiogram-gated cine imaging for the assessment of global und regional left ventricular function in clinical routine," *Eur. Radiol.*, vol. 22, no. 3, pp. 559–568, 2012.

[95] S. Maderwald *et al.*, "7 tesla cardiac imaging with a phonocardiogram trigger device," in *Proc. Int. Soc. Magn. Reso. Med.*, 2011, p. 1322.

[96] MRI.TOOLS GmbH, "MRI.TOOLS – Innovation for medical imaging," 2021. [Online]. Available: https://www.mritools.de/index.php/products/mri-accessories/easyact/

[97] A. C. Larson, R. D. White, G. Laub, E. R. McVeigh, D. Li, and O. P. Simonetti, "Self-gated cardiac cine MRI," *Magn. Reson. Med.*, vol. 51, no. 1, pp. 93–102, 2004.

[98] B. Hiba, N. Richard, M. Janier, and P. Croisille, "Cardiac and respiratory double self-gated cine MRI in the mouse at 7T," *Magn. Reson. Med.*, vol. 55, no. 3, pp. 506–513, 2006.

[99] G. M. Nijm, A. V. Sahakian, S. Swiryn, J. C. Carr, J. J. Sheehan, and A. C. Larson, "Comparison of self-gated cine MRI retrospective cardiac synchronization algorithms," *J. Magn. Reson. Imag.*, vol. 28, no. 3, pp. 767–772, 2008.

[100] M. E. Crowe *et al.*, "Automated rectilinear self-gated cardiac cine imaging," *Magn. Reson. Med.*, vol. 52, no. 4, pp. 782–788, 2004.

[101] T. A. Spraggins, "Wireless retrospective gating: Application to cine cardiac imaging," *Magn. Reson. Imag.*, vol. 8, no. 6, pp. 675–681, 1990.

[102] R. D. White, C. B. Paschal, M. E. Clampitt, T. A. Spraggins, and G. W. Lenz, "Electrocardiograph-independent, 'wireless' cardiovascular cine MR imaging," *J. Magn. Reson. Imag.*, vol. 1, no. 3, pp. 347–355, 1991.

[103] N. Gai and L. Axel, "Correction of motion artifacts in linogram and projection reconstruction MRI using geometry and consistency constraints," *Med. Phys.*, vol. 23, no. 2, pp. 251–262, 1996.

[104] C. J. Hardy, L. Zhao, X. Zong, M. Saranathan, and E. K. Yucel, "Coronary MR angiography: Respiratory motion correction with BACSPIN," *J. Magn. Reson. Imag.*, vol. 17, no. 2, pp. 170–176, 2003.

[105] M. Kachelrieß, D.-A. Sennst, W. Maxlmoser, and W. A. Kalender, "Kymogram detection and kymogram-correlated image reconstruction from subsecond spiral computed tomography scans of the heart," *Med. Phys.*, vol. 29, no. 7, pp. 1489–1503, 2002.

[106] J. M. Rubin, J. B. Fowlkes, M. R. Prince, R. T. Rhee, and T. L. Chenevert, "Doppler US gating of cardiac MR imaging," *Acad. Radiol.*, vol. 7, no. 12, pp. 1116–1122, 2000.

[107] F. Kording *et al.*, "Doppler ultrasound compared with electrocardiogram and pulse oximetry cardiac triggering: A pilot study," *Magn. Reson. Med.*, vol. 74, no. 5, pp. 1257–1265, 2015.

[108] F. Kording *et al.*, "Doppler ultrasound triggering for cardiovascular MRI at 3T in a healthy volunteer study," *Magn. Reson. Med. Sci.*, vol. 16, no. 2, pp. 98–108, 2017.

[109] Ultrasound Supply, "Ultrasound Supply - Ultrasounds, C-Arms, Probes," 2021. [Online]. Available: https://www.ultrasoundsupply.com/products/ultrasound-probes/ge-probes/pa6-8-cardiac-sector-probe/

[110] A. Taebi, B. Solar, A. Bomar, R. Sandler, and H. Mansy, "Recent advances in seismocardiography," *Vibration*, vol. 2, no. 1, pp. 64–86, 2019.

[111] O. T. Inan *et al.*, "Ballistocardiography and seismocardiography: A review of recent advances," *IEEE J. Biomed. Health Informat.*, vol. 19, no. 4, pp. 1414–1427, Jul. 2015.

[112] G. Cosoli, L. Casacanditella, E. P. Tomasini, and L. Scalise, "Heart rate assessment by means of a novel approach applied to signals of different nature," *J. Phys.: Conf. Ser.*, vol. 778, no. 1, pp. 1–8, 2017.

[113] F. Landreani *et al.*, "Beat-to-beat heart rate detection by smartphone's accelerometers: Validation with ECG," in *Proc. 38th Annu. Int. Conf. IEEE Eng. Med. Biol. Soc.*, 2016, pp. 525–528.

[114] M. J. Tadi *et al.*, "A real-time approach for heart rate monitoring using a hilbert transform in seismocardiograms," *Physiol. Meas.*, vol. 37, no. 11, pp. 1885–1909, 2016.

[115] A. Taebi, A. J. Bomar, R. H. Sandler, and H. A. Mansy, "Heart rate monitoring during different lung volume phases using seismocardiography," in *Proc. SoutheastCon*, 2018, pp. 1–5.

[116] M. J. Tadi, E. Lehtonen, O. Lahdenoja, M. Pankaala, and T. Koivisto, "An adaptive approach for heartbeat detection based on S-transform in seismocardiograms," in *Proc. 38th Annu. Int. Conf. IEEE Eng. Med. Biol. Soc.*, 2016, pp. 2370–2373.

[117] J. Wahlstrom *et al.*, "A hidden markov model for seismocardiography," *IEEE Trans. Biomed. Eng.*, vol. 64, no. 10, pp. 2361–2372, Oct. 2017.

[118] J. Yao, S. Tridandapani, W. F. Auffermann, C. A. Wick, and P. T. Bhatti, "An adaptive seismocardiography (SCG)-ECG multimodal framework for cardiac gating using artificial neural networks," *IEEE J. Trans. Eng. Health Med.*, vol. 6, no. 1, pp. 1–11, Oct. 2018.

[119] M. J. Tadi, T. Koivisto, M. Pänkäälä, and A. Paasio, "Accelerometer-based method for extracting respiratory and cardiac gating information for dual gating during nuclear medicine imaging," *Int. J. Biomed. Imag.*, vol. 2014, no. 1, pp. 1–11, 2014.

[120] M. Jerosch-Herold *et al.*, "The seismocardiogram as magnetic-field-compatible alternative to the electrocardiogram for cardiac stress monitoring," *Int. J. Cardiac Imag.*, vol. 15, no. 6, pp. 523–531, 1999.

[121] R. Martinek *et al.*, "A low-cost system for seismocardiography-based cardiac triggering: A practical solution for cardiovascular magnetic resonance imaging at 3 tesla," *IEEE Access*, vol. 7, pp. 118608–118629, 2019.

[122] SIEMENS AG, "SyngoMRE11 operator 1710 manual - body," [Online]. Available: https://cbbi.udel.edu/wp-content/uploads/2017/01/Body.pdf

[123] M. Zaitsev, J. Maclaren, and M. Herbst, "Motion artifacts in MRI: A complex problem with many partial solutions," *J. Magn. Reson. Imag.*, vol. 42, no. 4, pp. 887–901, 2015.

[124] J. P. Earls, V. B. Ho, T. K. Foo, E. Castillo, and S. D. Flamm, "Cardiac MRI: Recent progress and continued challenges," *J. Magn. Reson. Imag.*, vol. 16, no. 2, pp. 111–127, 2002.

[125] A. D. Scott, J. Keegan, and D. N. Firmin, "Motion in cardiovascular MR imaging," *Radiology*, vol. 250, no. 2, pp. 331–351, 2009.

[126] P. G. Danias and W. J. Manning, "MR navigators and their use in cardiac and coronary imaging," in *Coronary Magnetic Resonance Angiography*, 1st ed., New York, NY, USA: Springer-Verlag, 2002, pp. 219–227.

[127] S. K. Lemieux and G. H. Glover, "An infrared device for monitoring the respiration of small rodents during magnetic resonance imaging," *J. Magn. Reson. Imag.*, vol. 6, no. 3, pp. 561–564, 1996.

[128] T. Noponen *et al.*, "Spirometry based respiratory gating method for cardiac PET and MRI imaging," in *Proc. IEEE Nucl. Sci. Symp. Conf. Rec.*, 2008, pp. 4832–4834.

[129] S. S. Vasanawala and E. Jackson, "A method of rapid robust respiratory synchronization for MRI," *Pediatr. Radiol.*, vol. 40, no. 10, pp. 1690–1692, 2010.

[130] D. A. Feinberg *et al.*, "Hybrid ultrasound MRI for improved cardiac imaging and real-time respiration control," *Magn. Reson. Med.*, vol. 63, no. 2, pp. 290–296, 2010.

[131] C. Santelli *et al.*, "Respiratory bellows revisited for motion compensation: Preliminary experience for cardiovascular MR," *Magn. Reson. Med.*, vol. 65, no. 4, pp. 1097–1102, 2011.

[132] M. Fajkus *et al.*, "MR fully compatible and safe FBG breathing sensor: A practical solution for respiratory triggering," *IEEE Access*, vol. 7, pp. 123013–123025, 2019.

[133] H. Kandpal, R. Sharma, K. S. Madhusudhan, and K. S. Kapoor, "Respiratory-triggered versus breath-hold diffusion-weighted MRI of liver lesions: Comparison of image quality and apparent diffusion coefficient values," *Amer. J. Roentgenol.*, vol. 192, no. 4, pp. 915–922, 2009.

[134] J. N. Oshinski, L. Hofland, S. Mukundan, W. T. Dixon, W. J. Parks, and R. I. Pettigrew, "Two-dimensional coronary MR angiography without breath holding," *Radiology*, vol. 201, no. 3, pp. 737–743, 1996.

[135] H. C. M. van den Bosch *et al.*, "Free-breathing MRI for the assessment of myocardial infarction: Clinical validation," *Amer. J. Roentgenol.*, vol. 192, no. 6, pp. W 277–W281, 2009.

[136] K. Matsunaga, G. Ogasawara, M. Tsukano, Y. Iwadate, and Y. Inoue, "Usefulness of the navigator-echo triggering technique for free-breathing three-dimensional magnetic resonance cholangiopancreatography," *Magn. Reson. Imag.*, vol. 31, no. 3, pp. 396–400, 2013.

[137] C. Klessen *et al.*, "Magnetic resonance imaging of the upper abdomen using a free-breathing T2-weighted turbo spin echo sequence with navigator triggered prospective acquisition correction," *J. Magn. Reson. Imag.*, vol. 21, no. 5, pp. 576–582, 2005.

[138] C. J. Zech *et al.*, "High-resolution MR-imaging of the liver with T2-weighted sequences using integrated parallel imaging: Comparison of prospective motion correction and respiratory triggering," *J. Magn. Reson. Imag.*, vol. 20, no. 3, pp. 443–450, 2004.

[139] D. C. Peters, R. Nezafat, H. Eggers, C. Stehning, and W. J. Manning, "2D free-breathing dual navigator-gated cardiac function validated against the 2D breath-hold acquisition," *J. Magn. Reson. Imag.*, vol. 28, no. 3, pp. 773–777, 2008.

[140] B. Taouli *et al.*, "Diffusion-weighted imaging of the liver: Comparison of navigator triggered and breathhold acquisitions," *J. Magn. Reson. Imag.*, vol. 30, no. 3, pp. 561–568, 2009.

[141] A. C. Larson *et al.*, "Preliminary investigation of respiratory self-gating for free-breathing segmented cine MRI," *Magn. Reson. Med.*, vol. 53, no. 1, pp. 159–168, 2005.

[142] N. Jin, R. J. Lewandowski, R. A. Omary, and A. C. Larson, "Respiratory self-gating for free-breathing abdominal phase-contrast blood flow measurements," *J. Magn. Reson. Imag.*, vol. 29, no. 4, pp. 860–868, 2009.

[143] J. Liu, P. Spincemaille, N. C. F. Codella, T. D. Nguyen, M. R. Prince, and Y. Wang, "Respiratory and cardiac self-gated free-breathing cardiac CINE imaging with multiecho 3D hybrid radial SSFP acquisition," *Magn. Reson. Med.*, vol. 63, no. 5, pp. 1230–1237, 2010.

[144] S. Uribe *et al.*, "Whole-heart cine MRI using real-time respiratory self-gating," *Magn. Reson. Med.*, vol. 57, no. 3, pp. 606–613, 2007.

[145] S. Uribe, P. Beerbaum, T. S. Sørensen, A. Rasmusson, R. Razavi, and T. Schaeffter, "Four-dimensional (4D) flow of the whole heart and great vessels using real-time respiratory self-gating," *Magn. Reson. Med.*, vol. 62, no. 4, pp. 984–992, 2009.

[146] R. Wang *et al.*, "Wearable respiration monitoring using an in-line few-mode fiber Mach-Zehnder interferometric sensor," *Biomed. Opt. Exp.*, vol. 11, no. 1, pp. 316–329, 2020.

[147] F. Michler *et al.*, "A clinically evaluated interferometric continuous-wave radar system for the contactless measurement of human vital parameters," *Sensors*, vol. 19, no. 11, pp. 1–19, 2019.

[148] H. Di, S. Sun, and Y. Che, "Respiration measurement using fibre-optic deformation sensor," *J. Modern Opt.*, vol. 64, no. 6, pp. 639–645, 2016.

[149] S. Chen, F. Tan, Z. Huang, T. Yang, J. Tu, and C. Yu, "Non-invasive smart monitoring system based on multi-core fiber optic interferometers," in *Proc. Asia Commun. Photon. Conf.*, 2018, pp. 1–3.

[150] Y. Zhang, Z. Chen, and H. I. Hee, "Noninvasive measurement of heart rate and respiratory rate for perioperative infants," *J. Lightw. Technol.*, vol. 37, no. 11, pp. 2807–2814, Jun. 2019.

[151] Z. Chen *et al.*, "Monitoring respiration and cardiac activity during sleep using microbend fiber sensor: A clinical study and new algorithm," in *Proc. 36th Annu. Int. Conf. IEEE Eng. Med. Biol. Soc.*, 2014, pp. 5377–5380.

[152] T. Liu *et al.*, "Medical respiratory monitoring sensors based on microbend fiber loss," *Proc. SPIE*, vol. 10025, 2017, Art. no. 1002517.

[153] X. Guo, Z. Li, and D. Yan, "A bio-signal monitoring sensor based on the microbending effect of fiber," *IOP Conf. Ser.: Mater. Sci. Eng.*, vol. 612, no. 2, pp. 1–8, 2019.

[154] H.-F. Hu, S.-J. Sun, R.-Q. Lv, and Y. Zhao, "Design and experiment of an optical fiber micro bend sensor for respiration monitoring," *Sensors Actuators A: Phys.*, vol. 251, no. 1, pp. 126–133, 2016.

[155] L. T. D'Angelo, S. Weber, Y. Honda, T. Thiel, F. Narbonneau, and T. C. Luth, "A system for respiratory motion detection using optical fibers embedded into textiles," in *Proc. 30th Annu. Int. Conf. IEEE Eng. Med. Biol. Soc.*, 2008, pp. 3694–3697.

[156] A. Grillet *et al.*, "Optical fibre sensors embedded into medical textiles for monitoring of respiratory movements in MRI environment," *Proc. SPIE*, vol. 6619, 2007, Art. no. 66191R.

[157] J. Witt *et al.*, "Smart medical textiles with embedded optical fibre sensors for continuous monitoring of respiratory movements during MRI," *Proc. SPIE*, vol. 7653, 2010, Art. no. 76533B.

[158] J. Witt *et al.*, "Medical textiles with embedded fiber optic sensors for monitoring of respiratory movement," *IEEE Sensors J.*, vol. 12, no. 1, pp. 246–254, Jan. 2012.

[159] D. Lo Presti *et al.*, "A multi-parametric wearable system to monitor neck movements and respiratory frequency of computer workers," *Sensors*, vol. 20, no. 2, pp. 1–17, 2020.

[160] W. Ecke *et al.*, "A novel periodic macrobending hetero-core fiber optic sensor embedded in textile for respiratory movements' analysis," *Proc. SPIE*, vol. 9062, 2014, Art. no. 90620D.

[161] A. Issatayeva, A. Beisenova, D. Tosi, and C. Molardi, "Fiber-optic based smart textiles for real-time monitoring of breathing rate," *Sensors*, vol. 20, no. 12, pp. 1–16, 2020.

[162] D. Lau *et al.*, "Intensity-modulated microbend fiber optic sensor for respiratory monitoring and gating during MRI," *IEEE Trans. Biomed. Eng.*, vol. 60, no. 9, pp. 2655–2662, Sep. 2013.

[163] W.-J. Yoo *et al.*, "Development of respiration sensors using plastic optical fiber for respiratory monitoring inside MRI system," *J. Opt. Soc. Korea*, vol. 14, no. 3, pp. 235–239, Sep. 2010.

[164] M. Krej, P. Baran, and Ł. Dziuda, "Detection of respiratory rate using a classifier of waves in the signal from a FBG-based vital signs sensor," *Comput. Methods Prog. Biomed.*, vol. 177, pp. 31–38, 2019.

[165] L. Mendes Pereira *et al.*, "UTE-SENCEFUL: First results for 3D high-resolution lung ventilation imaging," *Magn. Reson. Med.*, vol. 81, no. 4, pp. 2464–2473, Nov. 2018.

[166] N. S. Higano *et al.*, "Retrospective respiratory self-gating and removal of bulk motion in pulmonary UTE MRI of neonates and adults," *Magn. Reson. Med.*, vol. 77, no. 3, pp. 1284–1295, 2017.

[167] J. Delacoste, J. Chaptinel, C. Beigelman-Aubry, D. Piccini, A. Sauty, and M. Stuber, "A double echo ultra short echo time (UTE) acquisition for respiratory motion-suppressed high resolution imaging of the lung," *Magn. Reson. Med.*, vol. 79, no. 4, pp. 2297–2305, 2018.

[168] J. F. Heidenreich *et al.*, "Functional MRI of the lungs using single breath-hold and self-navigated ultrashort echo time sequences," *Radiol.: Cardiothoracic Imag.*, vol. 2, no. 3, pp. 1–7, Jun. 2020.

[169] M. Tibiletti *et al.*, "Multistage three-dimensional UTE lung imaging by image-based self-gating," *Magn. Reson. Med.*, vol. 75, no. 3, pp. 1324–1332, 2016.